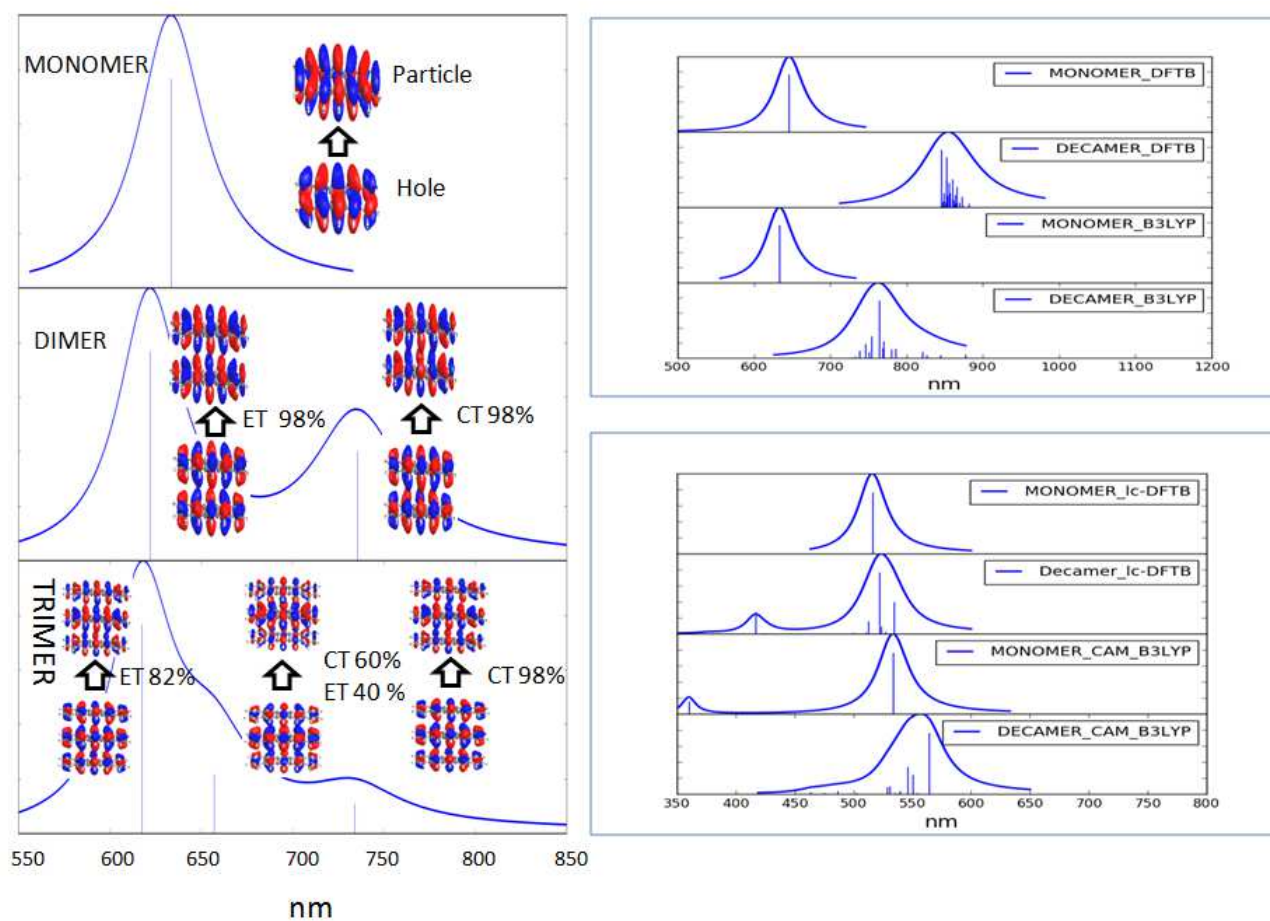


Davydov-Type Excitonic Effects on the Absorption Spectra of Parallel-Stacked and Herringbone Aggregates of Pentacene: Time-Dependent Density-Functional Theory and Time-Dependent Density-Functional Tight Binding

Ala Aldin M. H. M. Darghouth,^{*} Gabriela Calinao Correa [1],[†] Sacha Juillard,[,] and Mark E. Casida,[‡]
*Laboratoire de Chimie Théorique, Département de Chimie Moléculaire (DCM),
 Institut de Chimie Moléculaire de Grenoble (ICMG), Université Grenoble-Alpes,
 301 rue de la Chimie, CS 40700, 38058 Grenoble Cedex 9, France*

Alexander Humeniuk,[§] and Roland Mitrić[¶]
*Institut für Physikalische und Theoretische Chemie, Julius-Maximilians-Universität Würzburg,
 Emil-Fischer-Straße 42, D-97074 Würzburg, Germany*



Exciton formation leads to J-bands in solid pentacene. Describing these exciton bands represents a challenge for both time-dependent (TD) density-functional theory (DFT) and for its semi-empirical analogue, namely for TD density-functional tight binding (DFTB) for three reasons: (i) solid pentacene and pentacene aggregates are bound only by van der Waals forces which are notoriously difficult to describe with DFT and DFTB, (ii) the proper description of the long-range coupling between molecules, needed to describe Davydov splitting, is not easy to include in TD-DFT with traditional

functionals and in TD-DFTB, and (iii) mixing may occur between local and charge transfer excitons, which may, in turn, require special functionals. We assess how far TD-DFT and TD-DFTB have progressed towards a correct description of this type of exciton by including both a dispersion correction for the ground state and a range-separated hybrid functional for the excited state. Analytic results for parallel-stacked ethylene are derived which go beyond Kasha’s exciton model [Kasha, Rawls, and El-Bayoumi, *Pure Appl. Chem.* **11**, 371 (1965)] in that we are able to make a clear distinction between charge transfer and energy transfer excitons. This is further confirmed when it is shown that range-separated hybrids have a markedly greater effect on charge-transfer excitons than on energy-transfer excitons in the case of parallel-stacked pentacenes. TD-DFT calculations with the CAM-B3LYP functional and TD-*lc*-DFT calculations lead to negligible excitonic corrections for the herringbone crystal structure, possibly because of an overcorrection of charge-transfer effects. In this case, TD-DFT calculations with the B3LYP functional or TD-DFTB calculations parameterized to B3LYP give the best results for excitonic corrections for the herringbone crystal structure as judged from comparison with experimental spectra and with Bethe-Salpeter equation calculations from the literature. Oddly enough Kasha’s original formulation only seems to work when a range-separated functional is used in the case of off-set parallel pentacenes. This is traced back to a lack of consideration of avoided crossings in Kasha’s original formulation. Our improved model based upon nearest neighbor interactions does not suffer from this difficulty.

I. INTRODUCTION

Density-functional theory (DFT) has gained popularity for first-principles calculations of medium- to large-sized molecules or when large numbers of successive calculations are needed such as is the case for molecular dynamics. In fact, DFT has largely supplanted the older Hartree-Fock (HF) theory, except in cases where HF calculations are followed up by sophisticated post-HF correlated calculations. Although hybrid methods which integrate HF exchange into DFT have become popular, major Achilles heels of DFT have been dispersion forces and charge transfer phenomena. Likewise time-dependent (TD) DFT has become the dominant single-determinant-based approach for describing the excited states of medium- and large-sized molecules. But TD-DFT inherits many of the same problems as DFT, with a few more of its own [2, 3]. Density-functional tight-binding (DFTB) and TD-DFTB are semi-empirical versions, respectively, of DFT and of TD-DFT which (as should be expected from good approximations to DFT and to TD-DFT) inherit many of the problems from their first principles counterparts. General reliability and good scaling would seem to make DFT and TD-DFT (in the

first place) and DFTB and TD-DFTB (for still larger systems) excellent choices for atomistic modeling of organic electronics. However dispersion and charge transfer may or may not present real obstacles. The objective of this article is to take a look at the ability of modern DFT, TD-DFT, DFTB, and TD-DFTB to model aggregates of pentacene and solid pentacene. Our focus will be on intermolecular interactions in both the ground and in excited states.

Organic materials are typically bound together by some combination of hydrogen bonding and van der Waals forces. In the case of pentacene, the forces binding the molecules together are purely van der Waals in nature. It is thus imperative to be able to include dispersion forces. Traditional density functionals, such as the local density approximation (LDA), generalized gradient approximations (GGAs), meta-GGAs, and hybrid functionals fail to include the “action at a distance” aspect of dispersion forces because of their inability to give an accurate description of forces between molecules with nonoverlapping densities. Perhaps ironically, C_6 van der Waals coefficients — and hence dispersion forces — may be calculated accurately by TD-DFT. At this time, the most popular way to include dispersion forces in DFT calculations is to add on a semi-empirical correction [4] which is designed to interpolate between the DFT description of the charge density and the TD-DFT description of C_6 coefficients.

Organic electronics relies upon charge transport. However positive and negative carriers may be transported together in a charge-neutral packet called an exciton. From the condensed-matter point of view, excitons are born as

*ala.darghout@univ-grenoble-alpes.fr

†gcc73@cornell.edu

‡mark.casida@univ-grenoble-alpes.fr

§alexander.humeniuk@gmail.com

¶roland.mitric@uni-wuerzburg.de

local excitations. In fact, it is useful to make a distinction between “exciton structure” and “exciton dynamics” (p. 5 Ref. [5]). Although related to each other, exciton structure is more directly related to absorption spectra — the subject of the present article — while exciton dynamics falls more conveniently under the heading of charge and energy transport [6]. Even within the seemingly narrow subject of exciton structure, excitons seem to mean different things to different people. In particular, solid-state physicists may seem to require periodic (crystal) boundary conditions [5] in their definition of excitons, while chemists [7, 8] and biochemists [9] do not.

Here we focus on molecular solids where intermolecular interactions are important. Frenkel introduced the term “excitation packets” in his early study of the conversion of light into heat in solids [10, 11]. Unlike molecules which may often be considered to be small enough compared to the size of a photon that the photon may be approximated by an oscillating electric field, a solid is large compared to a photon. Moreover the crystal molecular orbitals should in principle extend over the entire crystal and so must also be large compared to the size of a photon. Yet experimental observations, and indeed common sense, suggests that photons may be absorbed locally. How may this observation be reconciled with the well-established concept of crystal molecular orbitals in periodic systems? Frenkel’s excitation packets resolved this apparent paradox by allowing the nearly degenerate crystal molecular orbitals to form wave packets whose size is on the order of one or several molecules and so for which photon absorption may be treated much like that of a molecule. This, in modern language, is the Frenkel exciton (FR). Another type of exciton — the Wannier-Mott exciton (WM) [12] — may be constructed for metals and semiconductors. Although not critical for the present work, it should be noted that FRs and WMs in periodic systems may be regarded as delocalized crystal states with a high conditional probability that, having specified the position of one charge, the other charge will then be found somewhere in the local neighborhood. The FRs and WMs form limiting cases, with real excitons being somewhere inbetween [5]. Thus, for a solid-state physicist, an exciton is a localized excitation which is small compared to a solid. A variation upon Frenkel excitons are Davydov excitons [13, 14] which will be discussed in the next paragraph.

Physical chemists and chemical physicists seem to have come across the exciton idea in a different way than did solid-state physicists, namely by noticing the appearance of new spectral features when certain dyes aggregate in

concentrated solution. If new very narrow peaks appear at lower energies, they are referred to as J-bands [15] (J for Jelly [16, 17] who, along with Scheibe [18, 19] were some of the first to investigate this phenomenon); if the new peaks appear at higher energies, they are referred to as H-bands (H for hypsochromic). Kasha and coworkers were able to give a convincing description of the origin of these bands in terms of the same ideas used by Davydov for solids [7, 8]. In particular, local excitons on different molecules interact in such a way as to lead to Davydov splitting (DS) of otherwise degenerate excitations. It is thus important to describe, not just *intramolecular* interactions correctly, but also to describe *intermolecular* interactions correctly, if the goal is to model J- or H-band DS. Several ways to improve the description of intermolecular interactions in DFT are available, including GGAs, global hybrids, and range-separated hybrids.

Yet another complication can arise as excitations need not be only within a single molecule (local excitation, LE), but rather may include excitations transferring charge from one molecule to a nearby molecule (charge transfer, CT). As FRs result from interacting LEs, one might think that CT could be ignored when modeling J- or H-bands. However this is not the case when CT and LEs mix, as is thought to occur in crystalline pentacene [20].

Time-dependent DFT with conventional functionals is notorious for underestimating CT excitations. This problem was clearly explained by Dreuw, Weisman, and Head-Gordon in their paper of 2003 [21] but was already apparent in an earlier paper by Tozer *et al.* in 1999 [22]. Later several diagnostic criteria were suggested to know when CT was likely to lead to a problem with TD-DFT with the best known one being the Λ criterion [23–29].

The situation in solid-state physics evolved somewhat differently beginning with the observation that the exact density functional must have some sort of ultranonlocality if atoms in the middle of a dielectric are to feel the effect of the field induced by charges on the surface of a dielectric. This led, for example, to the incorporation of current into TD-DFT [30]. The lack of ultranonlocality is often invoked to explain why TD-DFT calculations do not show exciton peaks in solid argon [31]. Sharma *et al.* proposed a bootstrap approximation to improve TD-DFT spectra for solids [32]. Ullrich and coworkers have discussed the problem of improving functionals for better description of excitons in crystal spectra [33–35]. The current recommendation to avoid the underestimation of CT excitations in TD-DFT is to use range-separated hybrids (RSHs) as these can “meet the challenge of CT

excitations” [36]. In fact, in their article of 2010, Wong and Hsieh argued strongly for the use of RSHs for the improvement of the description of excitons in the spectra of oligoacenes [37]. While encouraging, that study is also a bit misleading in the present context because it refers to excitons within a single covalently bonded molecule while our concern here is with excitonic effects on the spectra of aggregates held together by van der Waals forces. Nevertheless we concur on the importance of RSHs for describing excitons.

Two other approaches to describing excitonic effects with TD-DFT should be mentioned. This is subsystem TD-DFT [38, 39] which grew out of a little article by Casida and Wesolowski [40] showing how TD-DFT could be done on a subsystem of a larger system. The advantage of this method is that it incorporates the ideas of the exciton model from the very beginning as the system is viewed as made up of interacting chromophores. A different approach, albeit incorporating the exciton model from the very beginning, is used in Ref. 41. Note, however, that neither of these approaches are used in the present article. Instead, we emphasize obtaining excitonic effects from a supermolecule approach to van der Waals aggregates.

In the interest of future (and on-going) work on large and complex systems, our primary interest is in TD-DFTB. The present study seeks to find out how well state-of-the-art TD-DFTB calculations can mimic state-of-the-art TD-DFT calculations, including dispersion corrections and RSHs, for describing excitonic effects in pentacene aggregates. As an important goal is also understanding, we focus primarily on the overly simple case of parallel stacked pentacene molecules. However we then do go on and extend our tests to the known herringbone structure of solid pentacene which is an old, but still fairly popular, system in organic electronics [42] and which is known to show J-bands.

This paper is organized as follows. The next section reviews a minimum of basic theory needed for this paper. Sec. IV presents the details of how our computations were carried out and Sec. V presents and discusses our results. Sec. VI concludes.

II. EXCITON ANALYSIS

We have noticed that there seems to be a great deal of confusion in the literature regarding charge transfer in excitonic systems (e.g., see Ref. 43). Indeed delocalization of electron density over several molecules does not

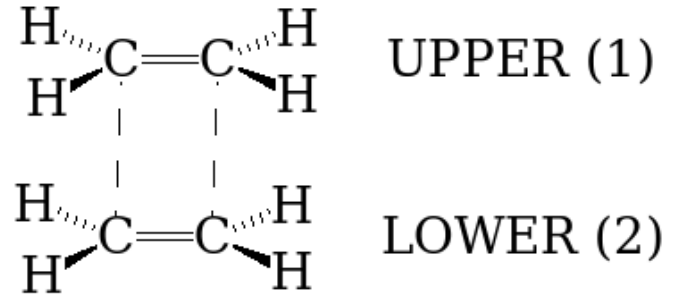


FIG. 1: Two vertically-stacked ethylene molecules.

necessarily imply excitonic charge transfer; what may be taken at first as an indication of charge transfer, may turn out to be a manifestation of energy transfer. For this reason, we wish to be especially careful to define these terms within the context of excitonic theory and, in particular, we seek to explain via an algebraic example how excitations described using MOs, delocalized over several molecules in a supermolecule, may be analyzed and understood in terms of the (mainly) pairwise interaction of excitations localized on different molecules to create ET and CT excitons. In particular, we wish to show algebraically and using chemical intuition to what extent Kasha’s exciton model [8] emerges from a linear combination of singly-excited determinants over MOs. For concreteness, we will treat the π system of vertically-stacked molecules of ethylene (Fig. 1). This is close enough to the case treated numerically in Sec. V that we will be able to use the equations developed for vertically-stacked ethylene to help understand the exciton physics of vertically-stacked pentacenes.

A. Monomer

The MOs of the π system of ethylene are shown in Fig. 2. MO symmetries have been assigned following the recommended International Union of Pure and Applied Chemistry (IUPAC) nomenclature [44, 45] and the symmetry of the expected lowest energy excitations have been assigned. Of particular importance for us is the sketch of the transition density $\psi_H(\mathbf{r})\psi_L(\mathbf{r})$ on the right-hand side of the figure with the associated transition dipole moment $\vec{\mu}_{HL}$. Here H stands for the highest occupied molecular orbital, while L stands for the lowest

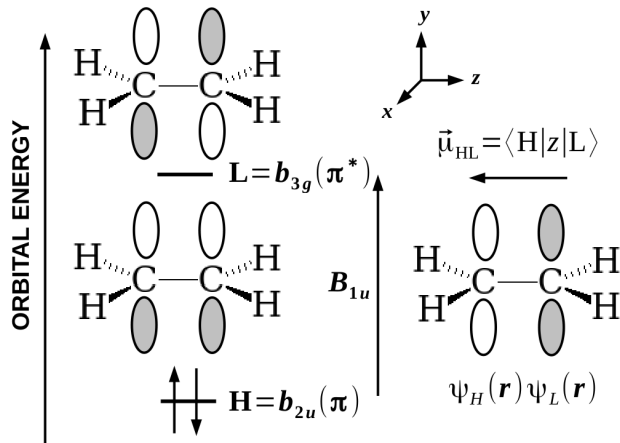


FIG. 2: Ethylene highest occupied molecular orbital (H) and lowest unoccupied molecular orbital (L).

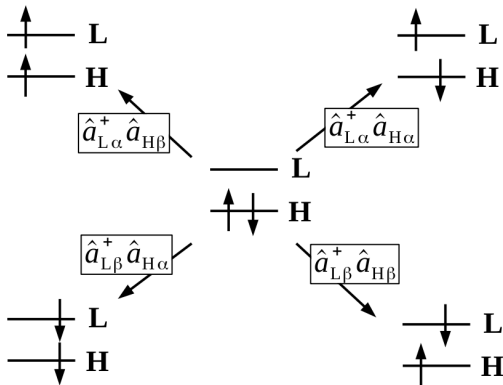


FIG. 3: Two-orbital two-electron model (TOTEM).

unoccupied molecular orbital.

This is evidently a two-orbital two-electron model (TOTEM, Fig. 3) and the excitations may be analyzed in this context. There are four possible one-electron excitations for the TOTEM, but spin symmetry must be taken properly into account. We shall focus on the singlet transition which goes from the ground-state determinant Φ

to the state,

$${}^1(H, L) = \frac{1}{\sqrt{2}} \left(\hat{a}_{L\alpha}^\dagger \hat{a}_{H\alpha} + \hat{a}_{L\beta}^\dagger \hat{a}_{H\beta} \right) \Phi, \quad (2.1)$$

where α and β refer to spin states (i.e., spin up and spin down, respectively). In the specific case of the TOTEM, we may just write

$$\begin{aligned} {}^1(H, L) &= \frac{1}{\sqrt{2}} (|H, \bar{L}\rangle + |L, \bar{H}\rangle) \\ &= \left[\frac{1}{\sqrt{2}} (H(1)L(2) + L(1)H(2)) \right] \\ &\times \left[\frac{1}{\sqrt{2}} (\alpha(1)\beta(2) - \beta(1)\alpha(2)) \right]. \end{aligned} \quad (2.2)$$

There are also three triplet states which are degenerate in the absence of spin-orbit coupling,

$$\begin{aligned} {}^3(H, L)_{M_S=+1} &= |H, L\rangle \\ &= \left[\frac{1}{\sqrt{2}} (H(1)L(2) - L(1)H(2)) \right] \\ &\times [\alpha(1)\alpha(2)] \\ {}^3(H, L)_{M_S=0} &= \frac{1}{\sqrt{2}} (|H, \bar{L}\rangle - |L, \bar{H}\rangle) \\ &= \left[\frac{1}{\sqrt{2}} (H(1)L(2) - L(1)H(2)) \right] \\ &\times \left[\frac{1}{\sqrt{2}} (\alpha(1)\beta(2) + \beta(1)\alpha(2)) \right] \\ {}^3(H, L)_{M_S=-1} &= |\bar{H}, \bar{L}\rangle \\ &= \left[\frac{1}{\sqrt{2}} (H(1)L(2) - L(1)H(2)) \right] \\ &\times [\beta(1)\beta(2)], \end{aligned} \quad (2.3)$$

which will not concern us here.

B. Dimer

We are now ready to treat two interacting stacked ethylene molecules. This system has been studied previously in the context of excitonic effects [46–49] and at a greater level of sophistication than that needed here. Instead, we try to keep our analysis as simple as possible by assuming weak interactions between the molecules so that we may go to trimers and oligomers. Thus the analysis in the present section is most correct only at large intermolecular distances.

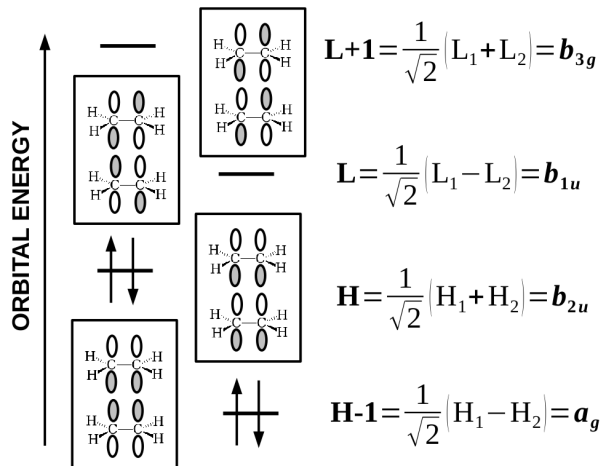


FIG. 4: MO diagram for two stacked ethylene molecules. White indicates the positive phase parts of the p functions while grey indicates the negative phase parts. Overlap between the MOs on different molecules have been neglected in normalizing the supermolecule MOs.

The corresponding dimer MO diagram (Fig. 4) under the assumption of weak interactions between the molecules. Here, after ordering MOs by energy, $H-n$ is the n th occupied MO below H and $L+n$ is the n th unoccupied MO above L . As expected the number of nodal planes also increases with MO energy. Although we might think of this as a four-orbital four-electron model, we would like to think in terms of the exciton model, which we shall refer to as (TOTEM)² for evident reasons. Both energy transfer (ET) and charge transfer (CT) excitons will emerge from our analysis.

Figure 5 shows the four possible singlet transitions in (TOTEM)² from the point of view of the MOs of the supermolecule composed of the two weakly-interacting ethylene molecules. Exciton analysis means that we want to re-express the description of the excitations so that they are no longer expressed in terms of the MOs of the supermolecule but rather are expressed in terms of ET and CT excitons involving the MOs (H_1 and L_1) of molecule 1 and the MOs (H_2 and L_2) of molecule 2. Figure 5 shows that the transitions divide neatly into two symmetry types, namely B_{1u} and B_{3g} . This simplifies our analysis as only orbitals of the same symmetry may mix.

Physically re-expressing supermolecule excitations in terms of ET and CT excitons on individual molecules

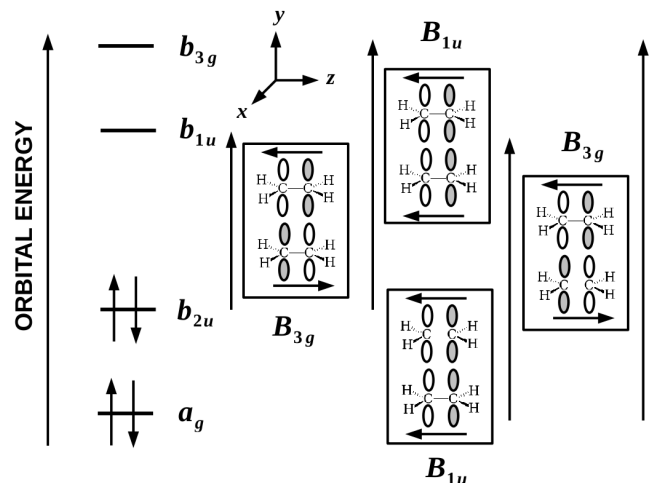


FIG. 5: The four transitions in (TOTEM)² and their associated transition dipole moments.

can only happen when there are enough degrees of liberty — and, in particular, quasidegenerate states — that delocalized orbitals can be re-expressed in terms of more localized orbitals. This does not happen for the B_{3g} transitions. In fact, the first B_{3g} transition is expected to be heavily dominated by the ${}^1(H, L)$ configuration and the remaining B_{3g} transition should be dominated by the ${}^1(H-1, L+1)$ configuration. However the B_{3g} transitions are spectroscopically dark. So we will just go directly on to the B_{1u} orbitals.

The most general B_{1u} transition is of the form,

$$\Psi = c_1 {}^1(H, L+1) + c_2 {}^1(H-1, L). \quad (2.4)$$

Expressing the aggregate MOs in terms of the local MOs of molecules 1 and 2 as given in Fig. 4 leads to,

$$\Psi = \frac{c_1 + c_2}{\sqrt{2}} \text{ET}_{12} + \frac{c_1 - c_2}{\sqrt{2}} \text{CT}_{12}, \quad (2.5)$$

where,

$$\text{ET}_{12} = \frac{1}{\sqrt{2}} [{}^1(H_1, L_1) + {}^1(H_2, L_2)] \quad (2.6)$$

is the pairwise ET exciton and,

$$\text{CT}_{12} = \frac{1}{\sqrt{2}} [{}^1(H_1, L_2) + {}^1(H_2, L_1)] \quad (2.7)$$

is the corresponding CT exciton. (See Fig. 6. Note that we make no attempt to distinguish between Förster

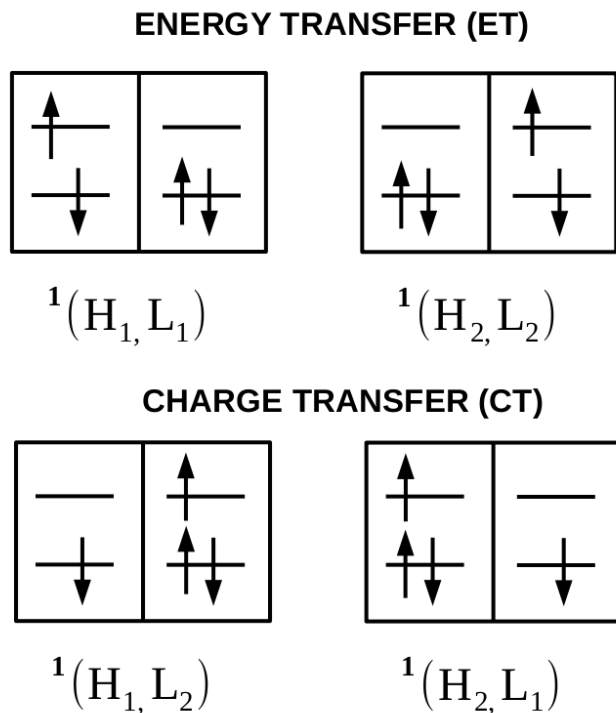


FIG. 6: Exciton model classification of transitions in the (TOTEM)² model. In each double box, the left hand side shows the orbital occupancy of the MOs in molecule 1 while the right hand side shows the orbital occupancy of the MOs in molecule 2.

and Dexter ET excitons.) Physically we expect the ${}^1(H-1, L)$ and ${}^1(H, L+1)$ transitions to be quasidegenerate (i.e., $c_1 \approx c_2$) as often happens in organic molecules with a conjugated π system. Kasha's theory is recovered for exact degeneracy (i.e., when $c_1 = \pm c_2 = 1/\sqrt{2}$). As Kasha's theory predicts significant oscillator strength, because of mutual reinforcement of the transition dipole moments of each molecule, we expect to see the monomer absorption peak blue-shifted to the new dimer ET_{12} absorption peak as shown in Fig. 7. It is split from dipole-forbidden CT_{12} peak in the dimer spectrum. The difference between the energies of the ET and CT states is the Davydov splitting ($DS = ET - CT$). Kasha's theory may be further developed to show a red shift upon the formation of head-to-tail dimers when the CT state is bright and the ET state is dark [8]. Other configurations yield two peaks with an experimentally observable DS whose relative intensities may be analyzed to give infor-

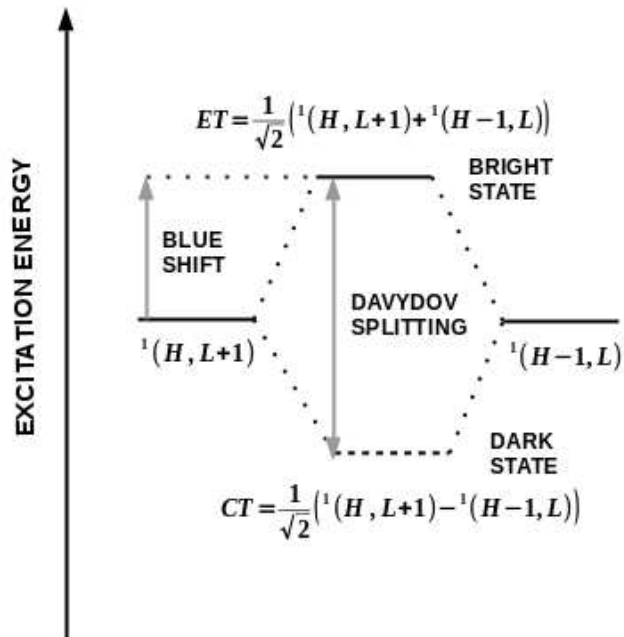


FIG. 7: Schematic of Kasha's theory for two parallel stacked molecules.

mation about the relative orientation of the molecules in the dimer [8].

C. Trimer

Three stacked trimers introduce another key level of complexity in the exciton model. We now have an interior molecule interacting with two outer molecules. This asymmetry means that transitions forbidden, and hence dark, in the dimer may now be allowed, and hence bright, in the trimer. Figure 8 shows the (TOTEM)³ MOs deduced by analogy with the simple Hückel solution for the propenyl radical.

Figure 9 show the nine single excitations. Only the five B_{1u} transitions are symmetry allowed for absorption spectroscopy. Figure 10 shows the transition densities for the five symmetry-allowed singlet transitions. We thus restrict our analysis to the linear combination of only these states,

$$\Psi = c_1 {}^1(H, L) + c_2 {}^1(H, L+2) + c_3 {}^1(H-1, L+1) + c_4 {}^1(H-2, L) + c_5 {}^1(H-2, L+2). \quad (2.8)$$

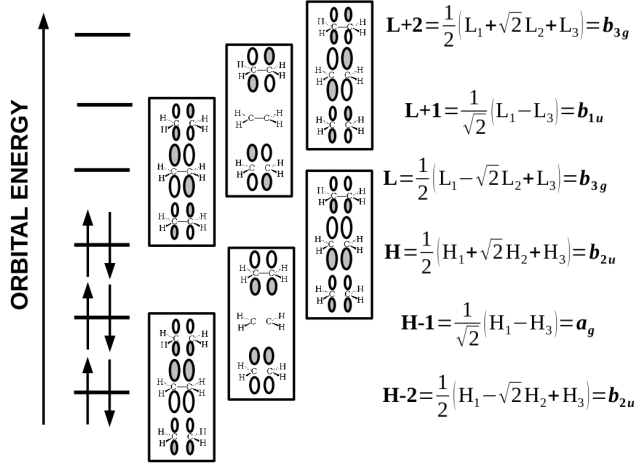


FIG. 8: MO diagram for three stacked ethylene molecules. White indicates the positive phase parts of the p functions while grey indicates the negative phase parts. Overlap between the MOs on different molecules have been neglected in normalizing the supermolecule MOs.

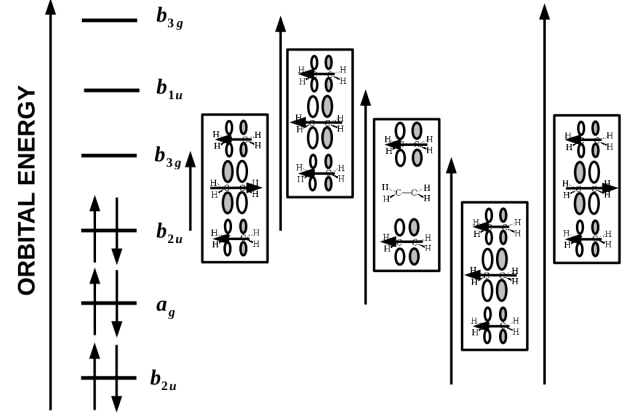


FIG. 10: The transition densities for the five symmetry allowed B_{1u} singlet excitations.

Furthermore, we will use chemical intuition to predict the general form of these five allowed transitions. In particular, only the ${}^1(H, L+2)$, ${}^1(H-1, H+1)$, and ${}^1(H-2, L)$ states are expected to be degenerate enough to mix to form pairwise ET and CT excitons. This gives, after some algebra,

$$\begin{aligned}
 \Psi = & c_1 {}^1(H, L) \\
 & + \frac{3c_2 + 2c_3 + 3c_4}{2\sqrt{6}} \left(\frac{\text{ET}_{12} + \text{ET}_{23}}{\sqrt{3}} \right) \\
 & + \sqrt{\frac{2}{3}} c_3 \left\{ \frac{\sqrt{3}}{2} \left[\text{ET}_{13} - \frac{1}{3} (\text{ET}_{12} + \text{ET}_{23}) \right] \right\} \\
 & + \frac{c_2 - c_4}{\sqrt{2}} \left(\frac{\text{CT}_{12} + \text{CT}_{23}}{\sqrt{2}} \right) \\
 & + \frac{c_2 - 2c_3 + c_4}{2\sqrt{2}} \text{CT}_{13} \\
 & + c_5 {}^1(H-2, L+2), \tag{2.9}
 \end{aligned}$$

where the notation is an obvious generalization of that given in Eqs. (2.6) and (2.7) and where the states have been orthonormalized. To a first approximation, the ${}^1(H, L)$ is too low in energy to mix with the other terms and ${}^1(H-2, L+2)$ is too high in energy to mix with the other terms. The ET and CT excitons lie in-between these in energy. Notice, however, that the CT terms vanish if $c_3 = c_4 = c_5$ which is expected to be often approximately the case. Note also that the pairwise ET

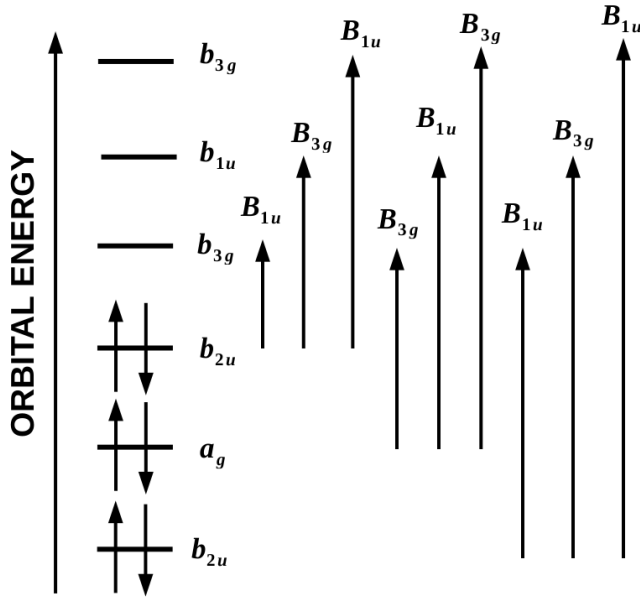


FIG. 9: The nine single excitations for three stacked ethylene molecules along with their symmetry assignments.

terms are *not* orthogonal to each other as, for example, $\langle \text{ET}_{12} | \text{ET}_{23} \rangle = \langle {}^1(H_2, L_2) | {}^1(H_2, L_2) \rangle / 2 = 1/2$. However the ET terms have been grouped to reflect the symmetry of the stack and the distance over which energy must be transferred.

As we shall see numerically in Sec. V for the trimer of stacked pentacene molecules, each term is a reasonably good first approximation to a calculated TD-DFT excitation. Notice the exceptions to Kasha’s model: (i) supermolecule MO excitations, such as ${}^1(H, L)$, which are better described in terms of supermolecule MOs than in terms of local MOs and (ii) CT excitons are only expected to cancel approximately in practical calculations. In reality ET and CT terms should mix.

The stacked trimer represents the simplest model where one molecule is interacting with two surrounding molecules. As such, it captures the basic physics of exciton interactions between neighboring molecules ($1 \leftrightarrow 2$ and $2 \leftrightarrow 3$). Equation (2.9) shows that neglect of $1 \leftrightarrow 3$ interactions (i.e., CT_{13} and ET_{13} and their required orthogonalization to the other terms) leads to only a single Davydov splitting into one ET and one CT peak. However a more careful analysis should include $1 \leftrightarrow 3$ interactions and Davydov multiplets may also be expected to be observed.

D. Higher Oligomers

The extension of these ideas to $(\text{TOTEM})^N$ for $N > 2$ is in principle straightforward but becomes increasingly complicated. However, it does not seem unreasonable to expect the structure of the spectrum to stabilize after a few layers, because the dominant interactions are expected to be primarily only between adjacent molecules. Thus we may anticipate that the numerical results in Sec. V should already show most of the qualitatively important features when $N = 3$ that are seen for still larger values of N .

We may explore this further by a back of the envelope tight-binding calculation for the periodic system of stacked ethylenes shown in Fig. 11. This is basically just a periodic simple Hückel calculation and so should be largely familiar to Quantum Chemists, even if the precise language and periodic symmetry adapted linear combinations may take a little getting used to.

To carry out our tight-binding calculation, we must include two ethylene molecules in the unit cell. In the exciton model, the MOs of each ethylene molecule $\chi_\mu(\vec{r})$ are looked on much like local AOs (LAOs). Combining

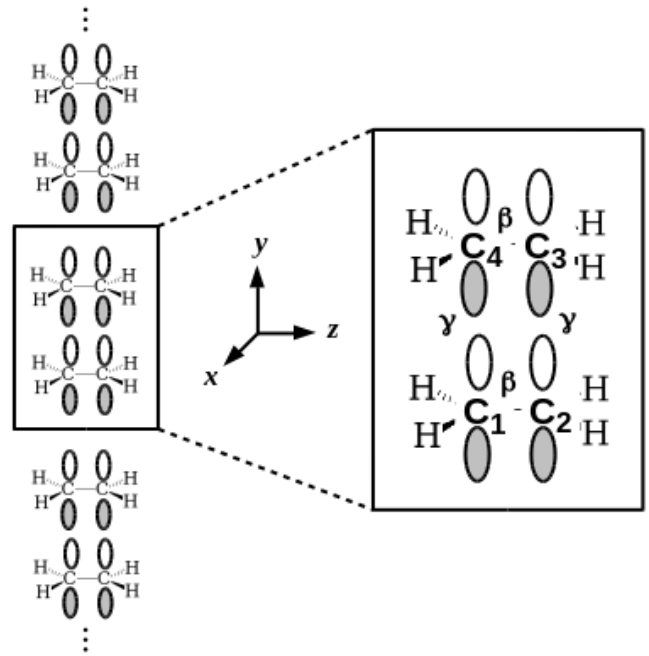


FIG. 11: Periodic model labeling and hopping parameters used for our stacked ethylene tight-binding calculation.

them gives us a set of $(\text{TOTEM})^2$ MOs which become local MOs (LMOs)

$$\psi_i(\vec{r}) = \sum_{\mu} \chi_{\mu}(\vec{r}) c_{\mu,i}. \quad (2.10)$$

Periodic symmetry-adapted linear combinations have the form of crystal MOs (CMOs)

$$\psi_i(\vec{r}; \vec{k}) = \sum_{\vec{R}} \psi_i(\vec{r} - \vec{R}) e^{i\vec{k} \cdot \vec{R}}, \quad (2.11)$$

which may also be written as,

$$\psi_i(\vec{r}; \vec{k}) = \sum_{\mu} \chi_{\mu}(\vec{r}; \vec{k}) c_{\mu,i}(\vec{k}), \quad (2.12)$$

in terms of crystal AOs (CAOs),

$$\chi_{\mu}(\vec{r}; \vec{k}) = \frac{1}{\sqrt{N}} \chi_{\mu}(\vec{r} - \vec{R}) e^{i\vec{k} \cdot \vec{R}}. \quad (2.13)$$

The factor N in this formalism represents the number of atoms in a fictitious “finite crystal.” It has been introduced for convenience, but it not really necessary. The

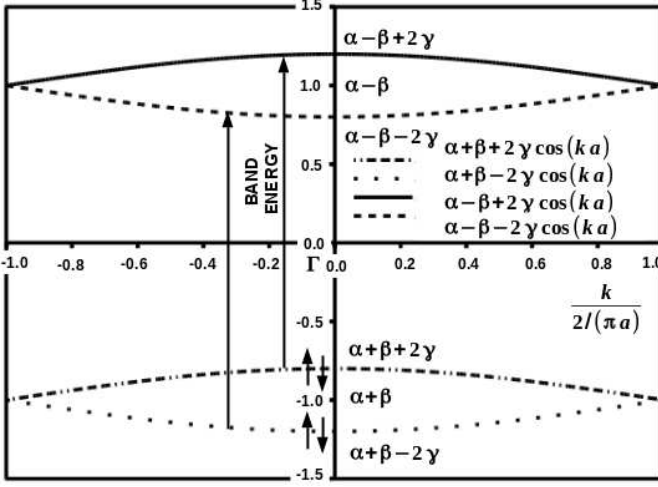


FIG. 12: Bands for the stacked ethylene tight-binding model with $\alpha = 0$, $\beta = -1$, and $\gamma = 0.1$. The paired arrows ($\uparrow\downarrow$) are meant to indicate filled bands below the fermi level.

wave vector \vec{k} serves both as a symmetry label and may also be viewed as a sort of electron momentum which can be used in selection rules. The \vec{k} -block of the CMO matrix equation is

$$\mathbf{h}(\vec{k})\vec{c}_i(\vec{k}) = \epsilon_i(\vec{k})\mathbf{s}(\vec{k})\vec{c}_i(\vec{k}), \quad (2.14)$$

where the matrix elements of the overlap matrix are given by,

$$s_{\mu,\nu}(\vec{k}) = \sum_{\vec{R}} s_{\mu,\nu}(\vec{R}) e^{i\vec{k}\cdot\vec{R}}$$

$$s_{\mu,\nu}(\vec{R}) = \int_{V=N\Omega} \chi_{\mu}^*(\vec{r} + \vec{R}) \chi_{\nu}(\vec{r}) d\vec{r}, \quad (2.15)$$

and the matrix elements of the hamiltonian matrix are given by,

$$h_{\mu,\nu}(\vec{k}) = \sum_{\vec{R}} h_{\mu,\nu}(\vec{R}) e^{i\vec{k}\cdot\vec{R}}$$

$$h_{\mu,\nu}(\vec{R}) = \int_{V=N\Omega} \chi_{\mu}^*(\vec{r} + \vec{R}) \hat{h} \chi_{\nu}(\vec{r}) d\vec{r}. \quad (2.16)$$

Here Ω is the volume of the unit cell and $N\Omega$ is the volume of the fictitious “finite crystal.”

Our model is subject to several simplifications. For one, the wave vector is a number k since our system is periodic in a single dimension (y). We will follow the

common practice of assuming that the overlap matrix $\mathbf{s}(k)$ is the identity. The hamiltonian matrix $\mathbf{h}(k)$ is then constructed from the on-sight (i.e., coulomb) integral α and the hopping (i.e., resonance) integrals β between the p orbitals within each ethylenes and γ between adjacent p orbitals in different ethylene molecules. Note that $\alpha, \beta < 0$ but that $\gamma > 0$ for this particular configuration. The position vector \vec{R} is Y so that

$$\mathbf{h}(k) = \sum_Y \mathbf{h}^{(Y)} e^{ikY}. \quad (2.17)$$

where,

$$\mathbf{h}^{(Y)} = \begin{bmatrix} \mathbf{A} & \mathbf{B} \\ \mathbf{C} & \mathbf{A} \end{bmatrix}$$

$$\mathbf{A} = \begin{bmatrix} \alpha\delta_{Y,0} & \beta\delta_{Y,0} \\ \beta\delta_{Y,0} & \alpha\delta_{Y,0} \end{bmatrix}$$

$$\mathbf{B} = \begin{bmatrix} 0 & \gamma(\delta_{Y,0} + \delta_{Y,+a}) \\ \gamma(\delta_{Y,0} + \delta_{Y,+a}) & 0 \end{bmatrix}$$

$$\mathbf{C} = \begin{bmatrix} 0 & \gamma(\delta_{Y,0} + \delta_{Y,-a}) \\ \gamma(\delta_{Y,0} + \delta_{Y,-a}) & 0 \end{bmatrix} \quad (2.18)$$

and a is the y -distance between ethylene molecules as opposed to the unit cell parameter which is equal to $2a$. Applying Eq. (2.17) to Eq. (2.18) then gives that

$$\mathbf{h}(k) = \begin{bmatrix} \mathbf{A} & \mathbf{B}(k) \\ \mathbf{C}(k) & \mathbf{A} \end{bmatrix}$$

$$\mathbf{A} = \begin{bmatrix} \alpha & \beta \\ \beta & \alpha \end{bmatrix}$$

$$\mathbf{B}(k) = \begin{bmatrix} 0 & \gamma(1 + e^{i2ka}) \\ \gamma(1 + e^{i2ka}) & 0 \end{bmatrix}$$

$$\mathbf{C}(k) = \begin{bmatrix} 0 & \gamma(1 + e^{-i2ka}) \\ \gamma(1 + e^{-i2ka}) & 0 \end{bmatrix}. \quad (2.19)$$

This has four solutions, namely:

$$\epsilon_1(k) = \alpha + \beta + 2\gamma \cos(ka) \leftrightarrow \vec{c}_1(k) = \begin{pmatrix} 1 \\ 1 \\ +z^*/|z| \\ +z^*/|z| \end{pmatrix}$$

$$\epsilon_2(k) = \alpha + \beta - 2\gamma \cos(ka) \leftrightarrow \vec{c}_2(k) = \begin{pmatrix} 1 \\ 1 \\ -z^*/|z| \\ -z^*/|z| \end{pmatrix}$$

$$\epsilon_3(k) = \alpha - \beta - 2\gamma \cos(ka) \leftrightarrow \vec{c}_3(k) = \begin{pmatrix} 1 \\ -1 \\ +z^*/|z| \\ -z^*/|z| \end{pmatrix}$$

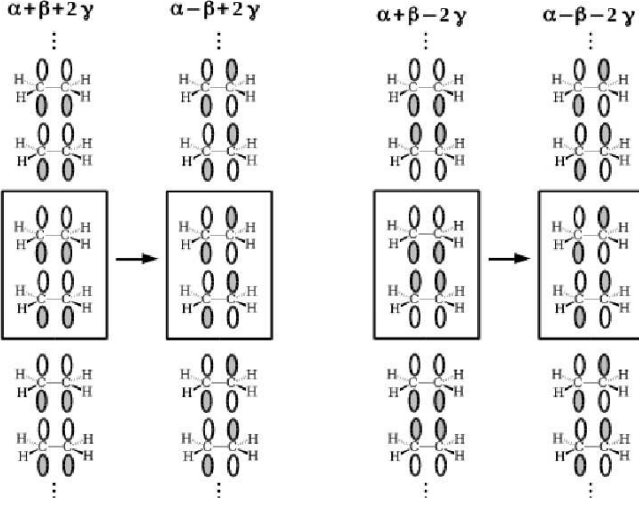


FIG. 13: The CMOs for the optically-allowed transitions of $(TOTEM)^N$ at the Γ -point.

$$\epsilon_4(k) = \alpha - \beta + 2\gamma \cos(ka) \leftrightarrow \vec{c}_4(k) = \begin{pmatrix} 1 \\ -1 \\ -z^*/|z| \\ +z^*/|z| \end{pmatrix}, \quad (2.20)$$

where,

$$z = 1 + e^{i2ka}. \quad (2.21)$$

The associated band diagram is shown in Fig. 12. This is a direct band system. Assuming the Γ point and no momentum transfer to the lattice, then the two allowed transitions are those shown by vertical arrows. The corresponding CMOs (Fig. 13) bear a close resemblance to the MOs of the $(TOTEM)^2$ dimer (Fig. 5), showing that the $(TOTEM)^2$ analysis also applies in the periodic $(TOTEM)^N$ case.

Finally, it is illuminating to apply the same tight-binding model to the $(TOTEM)^2$ dimer. The hamiltonian matrix to be diagonalized is then,

$$\mathbf{h}(k) = \begin{bmatrix} \mathbf{A} & \mathbf{B} \\ \mathbf{B} & \mathbf{A} \end{bmatrix} \quad (2.22)$$

$$\mathbf{A} = \begin{bmatrix} \alpha & \beta \\ \beta & \alpha \end{bmatrix}$$

$$\mathbf{B} = \begin{bmatrix} 0 & \gamma \\ \gamma & 0 \end{bmatrix},$$

which has the four solutions,

$$\begin{aligned} \epsilon_1 = \alpha + \beta + \gamma &\leftrightarrow \vec{c}_1 = \begin{pmatrix} 1 \\ 1 \\ 1 \\ 1 \end{pmatrix} \\ \epsilon_2 = \alpha + \beta - \gamma &\leftrightarrow \vec{c}_2 = \begin{pmatrix} 1 \\ 1 \\ -1 \\ -1 \end{pmatrix} \\ \epsilon_3 = \alpha - \beta - \gamma &\leftrightarrow \vec{c}_3 = \begin{pmatrix} 1 \\ -1 \\ 1 \\ -1 \end{pmatrix} \\ \epsilon_4(k) = \alpha - \beta + \gamma &\leftrightarrow \vec{c}_4 = \begin{pmatrix} 1 \\ -1 \\ -1 \\ 1 \end{pmatrix}. \end{aligned} \quad (2.23)$$

Comparing with the band solution for the periodic system $(TOTEM)^N$, we see that the energy levels are displaced by γ in $(TOTEM)^2$ rather than by 2γ in $(TOTEM)^N$, because each ethylene in $(TOTEM)^2$ is only in contact with a single other ethylene, while each ethylene in $(TOTEM)^N$ is in contact with two other ethylene molecules. However *the key energy differences are the same for $(TOTEM)^2$ and $(TOTEM)^N$* , lending reassurance that the fundamental analysis of the dimer model also applies for larger parallel stacks of ethylene molecules. On the other hand, inclusion of nonnearest neighbor interactions in the model is expected to yield small contributions from higher-order Davydov multiplets, even if our simple model captures the main qualitative aspects of Frenkel excitons in the stack of molecules.

This completes our analytic study of stacked ethylene dimers. In the Sec. V, we will apply this analysis to stacked pentamers and use it to gain a deeper insight into how different variations of TD-DFT and TD-DFTB work.

III. (TD-)DFT AND (TD-)DFTB

The previous formal section is important for our study of how well state-of-the-art TD-DFTB calculations can mimic state-of-the-art TD-DFT calculations. In this section, we will be more specific about what functionals are used in the present (TD-)DFT study and what (TD-)DFTB method was used. As we are testing existant methodology, rather than presenting new methodology,

this section is a review section. We will take advantage of this to keep our presentation brief (even just schematic) but will refer the reader back to the original literature or to important review articles. Hartree atomic units ($\hbar = m_e = e = 1$) are used throughout unless otherwise specified.

A. DFT

Hohenberg-Kohn-Sham DFT [50, 51] is now so well-known that little needs to be said about the basics. For those seeking a deeper understanding of the foundations of DFT, we can recommend Refs. 52–54. Our intent here is mainly to go beyond what is found in those references though some mention of the basics is inevitable.

The fundamental idea of DFT is to replace the real system of N interacting electrons in an external potential v_{ext} with a fictitious system of N noninteracting electrons in an effective potential v_s (s for single electron). We will designate the orbitals of the noninteracting system as ψ_i and their associated occupation numbers as n_i . These orbitals are orthonormal,

$$\langle \psi_i | \psi_j \rangle = \delta_{i,j}. \quad (3.1)$$

Normally n_i is zero or one but fractional occupation is also allowed. The density matrix for the noninteracting system is then,

$$\gamma(1, 2) = \sum_i \psi_i(1) n_i \psi_i^*(2), \quad (3.2)$$

where the numeral $i = 1, 2, \dots$ stands for the space and spin coordinates of the i th electron. The density,

$$\rho(1) = \gamma(1, 1). \quad (3.3)$$

is the diagonal element of the density matrix. The electronic energy E is the same for the real and for the interacting systems. It may be written as the sum of three terms,

$$E = E_c + E_H + E_{xc}, \quad (3.4)$$

where the core energy,

$$E_c = \sum_i n_i \langle \psi_i | \hat{h}_c | \psi_i \rangle, \quad (3.5)$$

may be expressed in terms of the core hamiltonian,

$$\hat{h}_c = -\frac{1}{2} \nabla^2 + v_{\text{ext}}, \quad (3.6)$$

the Hartree energy (also called the classical coulomb repulsion energy),

$$E_H = \frac{1}{2} \int \int \rho(1) \left(\frac{1}{r_{1,2}} \right) \rho(2) d1 d2, \quad (3.7)$$

and the remaining terms needed to make the electronic energy *exact* are included in the exchange-correlation (xc) energy,

$$E_{xc} = E - E_c - E_H. \quad (3.8)$$

This term is approximated in practical calculations. We will consider these approximations very soon. For now, let us note that minimizing E subject to the orthonormality condition [Eq. (3.1)] leads to an orbital equation,

$$\hat{f} \psi_i = \epsilon_i \psi_i, \quad (3.9)$$

where

$$\hat{f} = \hat{h}_c + v_H + v_{xc}. \quad (3.10)$$

Here

$$v_H(1) = \int \left(\frac{1}{r_{12}} \right) \rho(2) d2 \quad (3.11)$$

is the Hartree potential and

$$v_{xc}(1) = \frac{\delta E_{xc}}{\delta \rho(1)} \quad (3.12)$$

is the xc potential. Then it is easy to see that the effective potential of the noninteracting system is,

$$v_s = v_{\text{ext}} + v_H + v_{xc}. \quad (3.13)$$

The orbital equation (3.9) must be solved self-consistently because \hat{f} is orbital dependent. Once self-consistency has been reached, then the energy may be calculated either using Eq. (3.4) or by using the equation

$$E = \sum_i n_i \epsilon_i - \frac{1}{2} E_H + E_{xc} - \int v_{xc}(1) \rho(1) d1 \quad (3.14)$$

This latter form is used as the basis of DFTB.

Thus far the equations are exact, but useless unless approximations are made. The most common approximation is the local (spin) density approximation (LDA) which assumes that the xc energy density in a nonhomogeneous system such as an atom, molecule, or solid, is

the same as the xc energy density in the homogeneous electron gas (HEG),

$$E_{xc}^{\text{LDA}} = \int \epsilon_{xc}^{\text{HEG}}(\rho(1))\rho(1) d1. \quad (3.15)$$

The exchange part of $\epsilon_{xc}^{\text{HEG}}$ has a simple analytic form [55]. We will use the Vosko-Wilk-Nusair parameterization of the correlation part of $\epsilon_{xc}^{\text{HEG}}$ [56] in the present work. Strictly speaking all of our calculations have an explicit dependence on the spin polarization of the local density. That is, we are using spin DFT rather than the original DFT which depended only on the spinless charge density.

The LDA often gives reasonable molecular geometries but is known to overbind. For this reason, it has been useful to include inhomogeneities in the density via generalized gradient approximations (GGAs) of the form,

$$E_{xc}^{\text{GGA}} = \int \epsilon_{xc}^{\text{HEG}}(\rho(1))F_{xc}^{\text{GGA}}(\rho(1), x(1))\rho(1) d1. \quad (3.16)$$

where the enhancement factor F_{xc} depends both on the local density and upon the local reduced gradient,

$$x = \frac{|\vec{\nabla}\rho|}{\rho^{4/3}}. \quad (3.17)$$

Relevant GGAs used in our calculations are Becke’s 1988 (B88) exchange GGA [57, 58], Perdew’s 1991 correlation GGA [59–62], and the Lee, Yang, and Parr (LYP) correlation GGA [63].

Thus far, the discussion has been limited to pure density functionals — that is, those that depend only upon the charge density. In 1993, Becke introduced some “exact exchange” into the xc functional [64] (exact exchange is HF exchange evaluated with DFT orbitals.) He did this based upon an adiabatic connection formalism and the improvement in computational results was very striking in that time as they suggested that such (global) hybrid functionals could provide thermochemical accuracy. Of course, this also leaves the framework of formal Hohenberg-Kohn-Sham theory [65] and we must now speak of generalized Kohn-Sham theory. In particular, the xc energy is now a functional of the density matrix $E[\gamma]$ rather than just the density ($E[\rho]$) and the xc potential becomes an xc operator defined by

$$\hat{v}_{xc}\psi(1) = \int \frac{\delta E_{xc}}{\delta \gamma(2,1)}\gamma(1,2)\psi_i(2) d2. \quad (3.18)$$

TABLE I: Summary of different functionals used in this work. See Eq. (3.24).

Functional	μ	a_0	a_x	a_c
HF ^a	$+\infty$	1	0	0
LDA	0	0	0	1
B3LYP	0	0.20	0.72	0.81
CAM-B3LYP	0.33	0.19	0.46	0.81
LRC-LDA	0.4	0	1	0

^aIn the HF case, we also need to drop the E_c^{VWN80} term.

Note that the HF exchange-only operator may be regarded as an extreme case of a global hybrid:

$$E_x^{\text{HF}}[\gamma] = -\frac{1}{2} \int \int \gamma(1,2) \left(\frac{1}{r_{1,2}} \right) \gamma(2,1) d1d2$$

$$\frac{\delta E_x^{\text{HF}}[\gamma]}{\delta \gamma(2,1)} = -\frac{\gamma(1,2)}{r_{1,2}}. \quad (3.19)$$

Equation (3.14) still holds but with a nonlocal \hat{v}_{xc} . We use the B3LYP functional in the present work [66]. This is the same as the B3P91 functional originally introduced by Becke [64] but with Perdew’s 1991 correlation GGA replaced by the LYP correlation GGA. Specifically,

$$E_{xc} = E_x^{\text{LDA}} + a_0 (E_x^{\text{HF}} - E_x^{\text{LDA}}) + a_x E_x^{\text{B88}} + E_c^{\text{LDA}} + a_c (E_c^{\text{LYP}} - E_c^{\text{LDA}}), \quad (3.20)$$

where the various functionals have been defined above, $a_0 = 0.20$, $a_x = 0.72$, and $a_c = 0.81$.

We have emphasized that, in TD-DFT, charge-transfer excitations require the use of RSHs [36]. These functionals involve the splitting of the electron repulsion into a short-range (sr) and a long-range (lr) part,

$$\frac{1}{r_{12}} = \left(\frac{1}{r_{12}} \right)^{(\text{sr})} + \left(\frac{1}{r_{12}} \right)^{(\text{lr})}. \quad (3.21)$$

For convenience in a Gaussian orbital-based program, the separation is made using the error function,

$$\text{erf}(\mu r_{12}) = \frac{2}{\sqrt{\pi}} \int_0^{\mu r_{12}} e^{-t^2} dt. \quad (3.22)$$

We will be using the Coulomb attenuated model (CAM) B3LYP functional [67] where,

$$\left(\frac{1}{r_{12}} \right)^{(\text{sr})} = \frac{1 - [a_0 + a_x \text{erf}(\mu r_{12})]}{r_{12}}$$

$$\left(\frac{1}{r_{12}} \right)^{(\text{lr})} = \frac{a_0 + a_x \text{erf}(\mu r_{12})}{r_{12}}, \quad (3.23)$$

The sr part of the functional is treated by DFT while the lr part is treated by HF. The parameter μ acts as a range-separation parameter. The specific form of the CAM-B3LYP functional is,

$$E_{xc} = E_x^{\text{sr-LDA}} + a_0[E_x^{\text{lr-HF}} - E_x^{\text{sr-LDA}}] + a_x E_x^{\text{sr-B88}} + E_c^{\text{VWN80}} + a_c[E_c^{\text{LYP88}} - E_c^{\text{VWN80}}], \quad (3.24)$$

The specific parameters of the CAM-B3LYP functional are given in Table I. Also shown in the table are the values of the parameters which give some of the other functionals used in this paper. The LRC-LDA functional is the LDA form of the long-range corrected (LRC) functional of Iikura, Tsuneda, Yanai, and Harao [68]. This is given because the RSH DFTB used in this paper (*vide infra*) is based upon the LRC family of RSH functionals, rather than upon the CAM-B3LYP form.

The DFT presented thus far still has one very large failure, namely the lack of van der Waals (vdW) forces. This is particularly important in organic electronics because the organic molecules in the condensed phase are primarily held together precisely by these forces. However, to include vdW forces in *ab initio* theory, it is necessary to go beyond HF to at least second order in many-body perturbation theory (MBPT). Designing a density functional that can handle vdW forces has been studied and suggestions usually involve some aspect of MBPT. As TD-DFT resembles a MBPT method, it is perhaps not so remarkable that vdW coefficients for long-range induced-dipole/induced-dipole vdW forces can be calculated reasonably accurately via TD-DFT. The difficulty is then how to use TD-DFT (or some other MBPT approach) and make a computationally efficient method. The present method of choice, and the one used here, is actually a compromise. This is Grimme's D3 correction [4]. It has the semi-empirical form,

$$E_{\text{vdW}} = \sum_{A,B} \sum_{n=6,8,10,\dots} s_n \frac{C_n^{A,B}}{R_{A,B}^n \left[1 + 6 \left(\frac{R_{A,B}}{s_{r,n} R_0^{A,B}} \right)^{-\alpha_n} \right]} - \sum_{A,B,C} \frac{\sqrt{C_6^{A,B} C_6^{A,C} C_6^{B,C}} (3 \cos \theta_a \cos \theta_b \cos \theta_c + 1)}{(R_{A,B} R_{B,C} R_{C,A})^3 \left[1 + 6 \left(\frac{\bar{R}_{A,B,C}}{s_{r,3} R_0^{A,B}} \right)^{-\alpha_3} \right]}, \quad (3.25)$$

where the C_6 and other vdW coefficients are obtained from TD-DFT [see Ref. 4 for a more detailed description of the D3 correction and the values of the various

terms in Eq. (3.25)]. Thus this correction may be seen as an interpolation scheme between DFT and TD-DFT. However E_{vdW} enters as a correction which does not enter into the self-consistent cycle of orbital optimization but instead is added on, after the fact, as a first-order correction to the self-consistent field energy. Derivatives of E_{vdW} are included in force calculations and hence in geometry optimizations.

B. TD-DFT

TD-DFT is the younger sibling of DFT: The founding papers of DFT [50, 51] were written half a century ago; that of TD-DFT [69] a mere 30 years or so ago. The interested reader can find more information on TD-DFT in the proceedings of two summer schools on the topic [70, 71] as well as in two textbooks [72, 73] and in several recent review articles [2, 74–79].

The most common application of TD-DFT is to the calculation of electronic absorption spectra via response theory. There are several ways to do this, including real-time TD-DFT, but the classic approach is to use “Casida’s equation” (see, e.g., pp. 145-153 of the recent textbook, Ref. 73, or the original reference [80].) This method is about 20 years old. It consists of solving the pseudo-eigenvalue problem,

$$\begin{bmatrix} \mathbf{A} & \mathbf{B} \\ \mathbf{A}^* & \mathbf{B}^* \end{bmatrix} \begin{pmatrix} \vec{X} \\ \vec{Y} \end{pmatrix} = \omega \begin{bmatrix} \mathbf{1} & \mathbf{0} \\ \mathbf{0} & -\mathbf{1} \end{bmatrix} \begin{pmatrix} \vec{X} \\ \vec{Y} \end{pmatrix}, \quad (3.26)$$

where

$$\begin{aligned} A_{ia,jb} &= \delta_{i,j} \delta_{a,b} (\epsilon_a - \epsilon_i) + K_{ia,jb} \\ B_{ia,bj} &= K_{ia,bj} \end{aligned} \quad (3.27)$$

and the indices refer to excitations from occupied (i and j) to unoccupied (a and b) orbitals. The coupling matrix is usually evaluated in the adiabatic approximation, which leads to

$$\begin{aligned} K_{pq,rs} &= \int \int \int \int \psi_p^*(1) \psi_q(2) \\ &\times (f_H(1, 2; 3, 4) + f_{xc}(1, 2; 3, 4)) \\ &\times \psi_r(3) \psi_s^*(4) d1 d2 d3 d4, \end{aligned} \quad (3.28)$$

where,

$$\begin{aligned} f_H(1, 2; 3, 4) &= \delta(1-2) \frac{1}{r_{1,3}} \delta(3-4) \\ f_{xc}(1, 2; 3, 4) &= \frac{\delta E_{xc}}{\delta \gamma(2, 1) \delta \gamma(4, 3)}. \end{aligned} \quad (3.29)$$

The connection with the formal analysis of the previous section is most easily accomplished within the Tamm-Dancoff approximation (TDA),

$$\mathbf{A}\vec{X} = \omega\vec{X}. \quad (3.30)$$

The TDA makes TD-DFT look like configuration interaction with single excitations (CIS) which is exactly what it is when the TDA is applied to TD-HF. Many of the strengths and shortcomings of TD-DFT can be understood when the TDA is applied to the TOTEM to get the singlet excitation energy, ω_S . In the case of TD-HF,

$$\omega_S = \epsilon_L^{\text{HF}} - \epsilon_H^{\text{HF}} + 2(HL|f_H|LH) - (HH|f_H|LL), \quad (3.31)$$

where

$$(pq|f_H|rs) = \int \int \psi_p^*(1)\psi_q(1)\frac{1}{r_{1,2}}\psi_r^*(2)\psi_s(2) d1d2. \quad (3.32)$$

As Koopmans' theorem tells us that the HF orbital energies are better suited for describing ionization and electron attachment than for describing excitations, this is not such a good expression for local excitations. However it is well suited for describing CT excitations between two neutral molecules separated by a distance R as Eq. (3.31) becomes roughly the expected formula,

$$\omega_S = I - A - \frac{1}{R}, \quad (3.33)$$

as the ionization potential,

$$I \approx -\epsilon_H^{\text{HF}}, \quad (3.34)$$

and the electron affinity,

$$A \approx -\epsilon_L^{\text{HF}}, \quad (3.35)$$

while,

$$\begin{aligned} \lim_{R \rightarrow \infty} (HL|f_H|LH) &= 0 \\ \lim_{R \rightarrow \text{large}} (HH|f_H|LL) &\approx \frac{1}{R}. \end{aligned} \quad (3.36)$$

In contrast, for pure density functionals (LDA and GGAs),

$$\omega_S = \epsilon_L^{\text{DFT}} - \epsilon_H^{\text{DFT}} + 2(HL|f_H|LH) - (HL|f_{xc}^{\uparrow\uparrow} - f_{xc}^{\uparrow\downarrow}|LH), \quad (3.37)$$

where

$$(pq|f_{xc}|rs) = \int \int \psi_p^*(1)\psi_q(1)\frac{\delta E_{xc}}{\delta\rho(1)\delta\rho(2)}\psi_r^*(2)\psi_s(2) d1d2. \quad (3.38)$$

Since pure DFT orbitals see the same potential, and hence the same number of electrons, for both occupied and unoccupied orbitals, then the orbital energy difference is not a bad first approximation for local excitation energies. This provides an intuitive explanation of why TD-DFT often does better than TD-HF in this case. But, when we consider charge transfer between two widely separated molecules, Eq. (3.37) becomes

$$\lim_{R \rightarrow \text{large}} \omega_S \approx \epsilon_L^{\text{DFT}} - \epsilon_H^{\text{DFT}}, \quad (3.39)$$

which not only has the wrong R dependence but often grossly underestimates the difference between the ionization potential of one molecule and the electron affinity of the other.

Interestingly, exact TD-DFT with pure density functionals circumvents the CT problem by introducing a complicated frequency dependence into the xc kernel $f_{xc}(\omega)$ which imitates spatial nonlocality at particular values of ω . In particular, the time-dependent exchange-only optimized effective potential method gives [3, 81],

$$f_x(\epsilon_a - \epsilon_i) = (ai|f_H|ia). \quad (3.40)$$

While this formal result is highly interesting and can be implemented, the result is basically a very complicated DFT-like form of TD-HF. This suggests that it is better to introduce some exact exchange into our functionals, either through a global hybrid such as B3LYP or via a RSH such as CAM-B3LYP. The astute reader will note that the CAM-B3LYP functional has the wrong asymptotic behavior for CT excitations. Nevertheless, it remains a popular compromise for calculating excitation energies (e.g., see the DFT popularity poll [82]). However the LRC-type of RSH functional does have the correct asymptotic behavior and is the basis of the lc-DFTB functional described below.

C. DFTB

DFT scales formally as $\mathcal{O}(N^4)$ with the number of atoms N in the system. Depending upon the functional, its formal scaling may be reduced to $\mathcal{O}(N^3)$, but that still limits the usefulness of DFT. To go to still larger systems or resource intensive dynamics calculations, semi-empirical methods which use only $\mathcal{O}(N^2)$ integrals are useful.

Semi-empirical methods have a long history in quantum chemistry. Originally restricted to the π electrons

of conjugated systems, semi-empirical methods had been extended to all the valence electrons of a molecule by 1970 (the date of the classic text of Pople and Beveridge on this subject [83]). Ref. 84 provides a more up-to-date review of semi-empirical methods in quantum chemistry. A constant question with semi-empirical methods has been the physical meaning of the parameters used and how to assign them values. DFTB is specifically designed to approximate DFT with no more than two-centers integrals and no more than valence orbitals. In so doing, “the use of [DFT] removed at a stroke much of the problem of fitting parameters” [85]. The result resembles a less accurate (because less rigorous) form of DFT. Nevertheless the efficiency of DFTB makes it a highly desirable feature and most quantum chemistry packages include some form of DFTB. No attempt is made here to give a thorough review of all the different flavors of DFTB, but we will review the main points and refer the reader to the literature for additional information [86–88]. In particular, a very nice explanation of DFTB is given in Ref. 86.

The original form of DFTB [89], was a noniterative one-shot calculation resembling Hoffmann’s extended Hückel method [90–93]. The basis consists of the valence orbitals of isolated atoms calculated in a confining potential to ensure that those atomic orbitals remained local. It is important to keep track of the atom I on which resides the atomic orbital (AO) μ . We will denote this basis function as

$$\chi_{\mu I} = \chi_{\mu \in I}, \quad (3.41)$$

where the left-hand side is a shorter form of the right-hand side. The density is the superposition of atomic densities,

$$\rho_0 = \sum_I \rho_I^0. \quad (3.42)$$

The nuclear attraction term is separable,

$$v_{\text{ext}}[\rho_0] = \sum_I v_n[\rho_I^0], \quad (3.43)$$

and the Hartree potential is also separable,

$$v_H[\rho_0] = \sum_I v_H[\rho_I^0], \quad (3.44)$$

while the xc potential is assumed separable,

$$v_{\text{xc}}[\rho_0] = \sum_I v_{\text{xc}}[\rho_I^0], \quad (3.45)$$

which is a reasonable approximation for pure density functionals (LDA and GGAs). The matrix elements of the orbital hamiltonian (\hat{f}) are calculated as,

$$f_{\mu I, \nu J} = \begin{cases} \langle \chi_{\mu I} | \hat{t} + v_I^{nH_{\text{xc}}} | \chi_{\nu I} \rangle = \epsilon_I^0 & ; I = J \\ \langle \chi_{\mu I} | \hat{t} + v_I^{nH_{\text{xc}}} + v_J^{nH_{\text{xc}}} | \chi_{\nu J} \rangle & ; I \neq J \end{cases}, \quad (3.46)$$

where

$$\hat{t} = -\frac{1}{2}\nabla^2 \quad (3.47)$$

is the kinetic energy operator and

$$v_I^{nH_{\text{xc}}} = v_n[\rho_I^0] + v_H[\rho_I^0] + v_{\text{xc}}[\rho_I^0]. \quad (3.48)$$

This is known as the “potential superposition approximation.” A popular alternative is the “density superposition approximation” where $v_{\text{xc}}[\rho_I^0] + v_{\text{xc}}[\rho_J^0]$ is replaced with $v^{\text{xc}}[\rho_I^0 + \rho_J^0]$, hence reducing reliance on the assumption of a separable xc potential. Note that Eq. (3.47) involves only two-center integrals and

$$f_{\mu I, \nu I} = \delta_{\mu, \nu} \epsilon_{\mu I}^0, \quad (3.49)$$

where $\epsilon_{\mu I}$ is the AO energy for the isolated atom. This suffices for setting up the matrix form of the orbital equation,

$$\mathbf{f}\vec{c}_i = \epsilon_i \mathbf{s}\vec{c}_i, \quad (3.50)$$

and hence to calculate the band structure (BS) part of the total energy,

$$E_{\text{BS}} = \sum_i n_i \epsilon_i. \quad (3.51)$$

Of course, this neglects important terms on the right-hand side of Eq. (3.14), known in DFTB as the repulsion energy,

$$E_{\text{rep}} = -\frac{1}{2}E_H + E_{\text{xc}} - \int v_{\text{xc}}(1)\rho(1) d1. \quad (3.52)$$

It is a fundamental tenant of DFTB that this energy can be expanded as a set of pairwise potentials between different atom types,

$$E_{\text{rep}} = \sum_{I < J} V_{I, J}(R_{I, J}). \quad (3.53)$$

Finding and tabulating good transferable pair repulsion potentials $V_{I, J}(R_{I, J})$ is a major part of DFTB.

An important extension of DFTB is the addition of a self-consistent charge (SCC) term, E_{coul} , accounting for charge density corrections $\delta\rho$ beyond the original superposition of atomic densities approximation ρ_0 . This correction may be through second- [94] or third-order [95]. For simplicity, we describe only the second-order correction here. We seek a semi-empirical approximation to

$$E_{\text{coul}} = \frac{1}{2} \int \int \delta\rho(1) (f_H(1,2) + f_{xc}(1,2)) \delta\rho(2) d1d2. \quad (3.54)$$

This is accomplished by extensive use of two approximations. The first is Mulliken's approximation for use in approximating electron repulsion integrals (ERIs) [96],

$$\chi_{\mu I}^*(1)\chi_{\nu J}(1) \approx \frac{s_{\mu I, \nu J}}{2} (\chi_{\mu I}^*(1)\chi_{\mu I}(1) + \chi_{\nu J}^*(1)\chi_{\nu J}(1)), \quad (3.55)$$

which leads to

$$\psi_r^*(1)\psi_s(1) \approx \sum_{\mu I} q_{\mu I}^{r,s} \chi_{\mu I}^*(1)\chi_{\mu I}(1), \quad (3.56)$$

where

$$q_{\mu I}^{r,s} = \frac{1}{2} \sum_{\nu J} (c_{\mu I, r}^* s_{\mu I, \nu J} c_{\nu J, s} + c_{\mu I, s} s_{\mu I, \nu J} c_{\nu J, r}^*) \quad (3.57)$$

is a Mulliken transition charge. The second approximation is the gamma approximation

$$\chi_{\mu I}^*(1)\chi_{\mu I}(1) \approx g_I(1), \quad (3.58)$$

where g_I is an s -type function centered on atom I . The restriction to s -type functions is needed to solve a classic rotational invariance problem in semi-empirical theories (pp. 60-63 of Ref. [83]). (In more recent programs, g_I may be replaced with s -type functions g_{II} , allowing g_{II} to be different for different values of the angular momentum quantum number of $\chi_{\mu I}$ [97].) Together Mulliken's ERI approximation and the gamma approximation lead to the auxiliary-function expansion

$$\psi_r^*(1)\psi_s(1) \approx \sum_I q_I^{r,s} g_I(1), \quad (3.59)$$

where

$$q_I^{r,s} = \sum_{\mu \in I} q_{\mu I}^{r,s}. \quad (3.60)$$

The name "gamma approximation" comes from the integral,

$$\gamma_{I,J} = \int \int g_I(1) (f_H(1,2) + f_{xc}(1,2)) g_I(2) d1d2, \quad (3.61)$$

where,

$$f_H(1,2) = \frac{1}{r_{1,2}}$$

$$f_{xc}(1,2) = \frac{\delta^2 E_{xc}}{\delta\rho(1)\delta\rho(2)}, \quad (3.62)$$

which means that the density is

$$\rho(1) = \sum_i n_i \psi_i^*(1)\psi_i(1) \approx \sum_I q_I g_I(1), \quad (3.63)$$

where the Mulliken charge on atom I is

$$q_I = \sum_{\mu \in I} q_{\mu I}^{i,i} n_i. \quad (3.64)$$

The second-order SCC becomes

$$E_{\text{coul}}(\mathbf{R}) = \frac{1}{2} \sum_{I,J} \gamma_{I,J}(R_{I,J}) \Delta q_I \Delta q_J. \quad (3.65)$$

where Δq_I is the Mulliken charge fluctuation on atom I because

$$\delta\rho(1) \approx \sum_I \Delta q_I g_I(1). \quad (3.66)$$

Sometimes the diagonal elements $\gamma_{I,I}$ are calculated using some variation on Pariser's observation [98] that it should be equal to the difference between the ionization potential and electron affinity of atom I . This suggests that DFTB may work particularly well for calculating ionization potentials and electron affinities and this does seem to be the case [99], although the cited reference points out that DFTB was not parameterized to fit a single specific property, but rather to behave like DFT across a broad range of properties.

The SCC correction to the orbital hamilonian matrix,

$$f_{\mu I, \nu J} = \frac{s_{\mu I, \nu J}}{2} \sum_K (\gamma_{J,K} + \gamma_{K,I}) \Delta q_K, \quad (3.67)$$

is obtained in the usual way by variational minimization of the energy,

$$E = E_{\text{BS}} + E_{\text{rep}} + E_{\text{coul}} + E_{\text{vdW}}. \quad (3.68)$$

Note that we have added Grimme's D3 vdW correction to the DFTB energy formula as this is an important addition used in the present paper. Adding in this vdW term requires no essential changes in the DFTB formalism.

The construction of global hybrid and RSH versions of DFTB is now straightforward with appropriate modifications of the gamma integral. For example, to make the HF form of DFTB, both the xc parts of $E_{\text{BS}}[\rho_0]$ and of $E_{\text{rep}}[\delta\rho]$ must be replaced by the semi-empirical forms:

$$\begin{aligned}\gamma_{I,J} &= \int \int g_I(1) f_H(1,2) g_J(2) d1d2, \\ J &= \sum_{i,j} n_i \langle ii | f_H | jj \rangle n_j = \sum_{I,J} q_I \gamma_{I,J} q_J, \\ K &= \sum_{i,j} n_i \langle ij | f_H | ji \rangle n_j = \sum_{I,J} \gamma_{I,J} \left(\sum_{i,j} n_k q_I^{i,j} q_J^{j,i} n_j \right).\end{aligned}\quad (3.69)$$

The first version of RSH DFTB seems to be that of Niehaus and Della Sella [100]. This was followed by an implementation by Niehaus [101] (see also Ref. 102) and by Humeniuk and Mitrić [103, 104]. We will be using the latter form which was parameterized to behave like a LRC version of their DFTB method which, itself, was parameterized to behave like PBE DFT. We will refer to the resultant method as lc-DFTB following Humeniuk and Mitrić and we will see that it behaves not unlike CAM-B3LYP DFT. The long-range γ -matrix is given by,

$$\gamma_{I,J}^{\text{lr}}(R_{I,J}; \mu) = \text{erf}(\mu R_{I,J}) \gamma_{I,J}(R_{I,J}), \quad (3.70)$$

where $\mu = 1/R_{\text{max}}$ is the usual range-separation parameter. Humeniuk and Mitrić also neglect the long-range contribution to E_{BS} on the grounds that the zero-order system “already accounts for all interactions between electrons in the neutral atoms” [104].

D. TD-DFTB

Niehaus *et al.* were the first to extend DFTB to TD-DFTB [97, 105–107]. This is greatly facilitated by the observation that the TD-DFT coupling matrix is already approximated in the E_{coul} term of TD-DFTB. This allows the \mathbf{A} and \mathbf{B} matrices in Casida’s equation to be written out in TD-DFTB form. The TD-DFTB coupling matrix is given by

$$K_{pq,rs} = \sum_{I,J} q_I^{p,q} \gamma_{I,J} q_J^{s,r}, \quad (3.71)$$

with $\gamma_{I,J}$ defined as in Eq. (3.61). For a detailed treatment of spin and separation into singlet and triplet

blocks, see e.g., Ref. [108]. The dipole matrix elements needed to calculate oscillator strengths are calculated as

$$\langle \psi_p | \vec{r} | \psi_q \rangle = \sum_I \vec{R}_I q_I^{p,q}. \quad (3.72)$$

Other implementations include that of Ref. 109. We will be using the TD-lc-DFTB described in Refs. 103, 104.

IV. COMPUTATIONAL DETAILS

Two programs were used to carry out the calculations reported in this paper, namely GAUSSIAN09 [110] for DFT and TD-DFT calculations and DFTBABY [103, 104] for DFTB and TD-DFTB calculations. Note that, although GAUSSIAN09 does have the ability to carry out DFTB calculations, only DFTBABY allows us to carry out state-of-the-art TD-lc-DFTB calculations. We will first describe the options used with each program in more detail. We will then go on to describe how the programs were used in structural and spectral studies.

GAUSSIAN09 [110] calculations may be described in terms of a “theoretical model” (p. 5, Ref. 111) which is fully specified, in our case, by indicating for an excited-state (i.e., TD) calculation, the choice of functional and the orbital basis set. This is conveniently expressed in expanded notation as

$$\text{(TD-)DFA1/Basis1//DFA2/Basis2}$$

(p. 96, Ref. 111), where DFA2 is the density-functional approximation used for the geometry optimization and Basis2 is the corresponding basis set used for the geometry optimization, and DFA1 is the density-functional approximation used for the TD-DFT calculation and Basis1 is the corresponding orbital basis used in the TD-DFT calculation. The density-functionals used (LDA, B3LYP, HF, CAM-B3LYP with or without Grimme’s D3 correction) were described in the previous section. Two orbital basis sets were used here, namely the the minimal STO-3G basis set [112, 113] and the much more flexible 6-31G(d,p) split-valence (hydrogen [114], carbon [115]) plus polarization basis set [116]. An example of the expanded notation is that TD-CAM-B3LYP/6-31G(d,p)//D3-CAM-B3LYP/6-31G(d,p) means that the geometry of the molecule was optimized using the 6-31G(d,p) basis set using the CAM-B3LYP functional with the D3 dispersion correction. Then a TD-DFT calculation was carried out at that geometry using the 6-31G(d,p) orbital basis set and the CAM-B3LYP functional. Often we will use a shorter nomenclature when

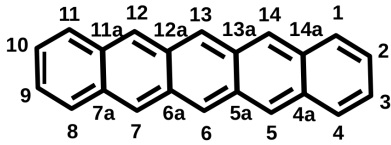


FIG. 14: Pentacene carbon numbering.

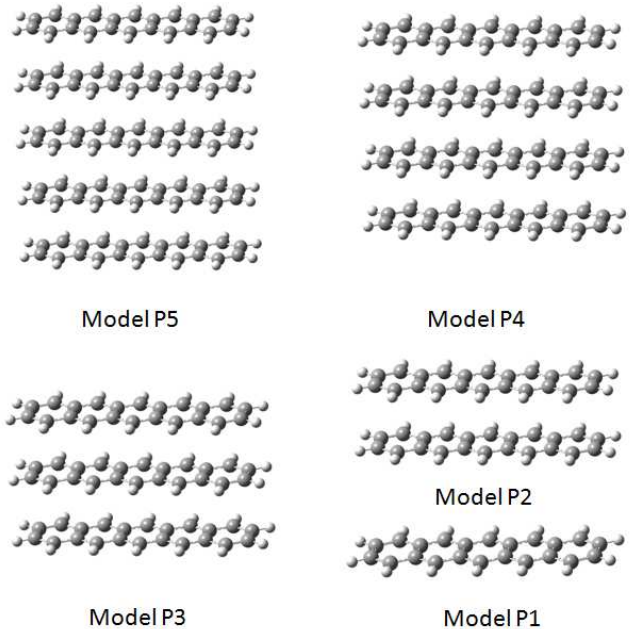
the details of the theoretical model are clear from context.

DFTBABY [103, 104] was used to carry out lc-DFTB and TD-lc-DFTB calculations. The values for the confinement radius r_0 and the Hubbard parameter U_H that were used to parameterize the electronic part of DFTB are shown in Table I of Ref. 103. The parameter for the lc correction was set to $R_{lc} = 3.03$ bohr so $\mu = 1/R_{lc} = 0.33$, which is a reasonable compromise between $\mu = 0.33$ used in the CAM-B3LYP functional and $\mu = 0.4$ used in the LRC family of functionals.

Our structural calculations started with initial x-ray crystallography geometries taken from the Crystallography Open Database (COD) [117, 118]. We will use the standard numbering of pentacene carbon shown in Fig. 14. We first optimized the *monomer* geometry and calculated its absorption spectrum at each level. Vibrational frequencies were calculated to make sure that the optimized structures were true minima. We then went on to study an ideal *parallel stacked* model in which B3LYP/6-31G(d,p) optimized monomers were π -stacked vertically face-to-face with a fixed distance R between them (Fig. 15). The distance R was optimized for the tetramer using different methods and then this distance was used in studying stacks of different sizes. Finally we studied calculated absorption spectra for cluster models cut out of the experimental *herringbone* structure without any geometry optimization.

V. RESULTS

Our goal in this section is to evaluate state-of-the-art (TD-)DFTB calculations of excitons in pentacene aggregates with state-of-the-art (TD-)DFT calculations on the same systems. We would also like to get a feeling for the relative importance of ET versus CT excitons. This involves three levels of calculation on three classes of systems. The three levels of calculation are first high-quality (TD-)DFT/6-31G(d,p) calculations aimed at obtaining good quality reference calculations which can be com-

FIG. 15: The configurations of the five models of parallel stacked pentacene (P_n stands for n parallel stacked pentacenes).

pared to experiment as a reality check. The second type of calculation consists of minimum basis set (TD-)DFT/STO-3G calculations as our ultimate goal is to evaluate the third method, namely the minimal basis set semi-empirical (TD-)DFTB method. The systems considered are first an isolated gas phase pentacene molecule, second a series of parallel stacked pentacene molecules as these parallel the theory already presented in Sec. II, and lastly a subunit of the known structure of crystalline pentacene.

A. Monomer

Although our primary interest here is in the absorption spectrum of the monomer, it is useful to begin with a review of the molecular orbitals (MOs). Figure 16 shows the result of a simple Hückel MO calculation with the SHMO calculator [119]. MO symmetries have been assigned following the recommended IUPAC nomenclature [44, 45] and the symmetry of the expected lowest energy excitations have been assigned.

The monomer geometry has been optimized at

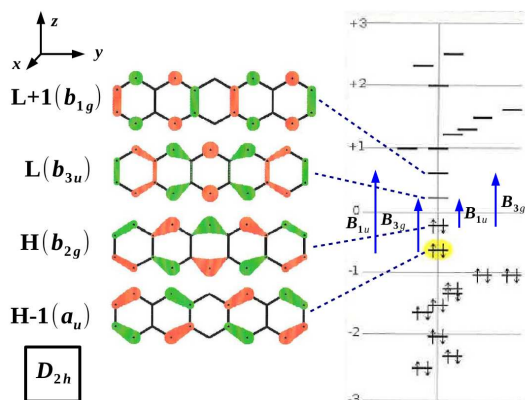


FIG. 16: Simple Hückel molecular orbital theory results for the pentacene monomer.

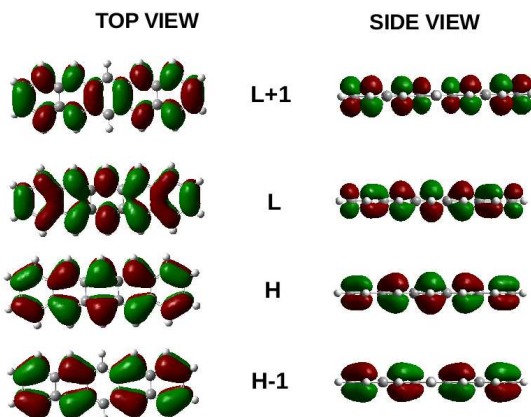
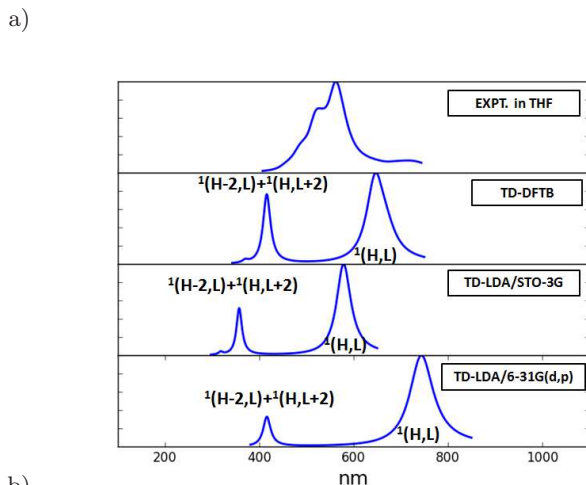


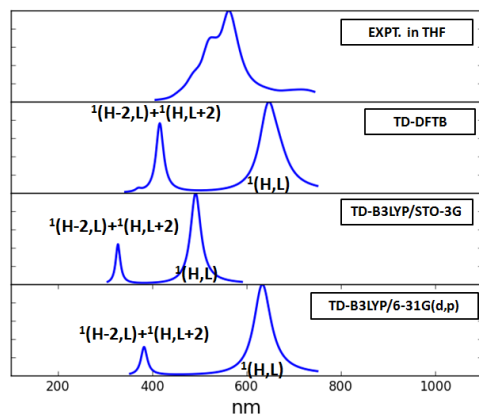
FIG. 17: Pentacene monomer B3LYP/6-31G(d,p) MOs.

the LDA/STO-3G, LDA/6-31G(d,p), B3LYP/STO-3G, B3LYP/6-31G(d,p), CAM-B3LYP/STO-3G, CAM-B3LYP/6-31G(d,p), DFTB, and lc-DFTB levels of theory. The orbitals at the resultant optimized geometries have been visualized (e.g., Fig. 17) and are found to be qualitatively similar to those obtained from simple Hückel MO theory. This is important as it is then relatively easy to make a connection between the results of stacked pentacene molecules and the theoretical discussion of Sec. II for stacked ethylene molecules.

Figure 18 compares the calculated monomer absorption spectra with the experimental spectrum measured in tetrahydrofuran (data obtained by plot digitization [120] of Fig. 1 of Ref. 121). Note that TD-DFT and



b)



c)

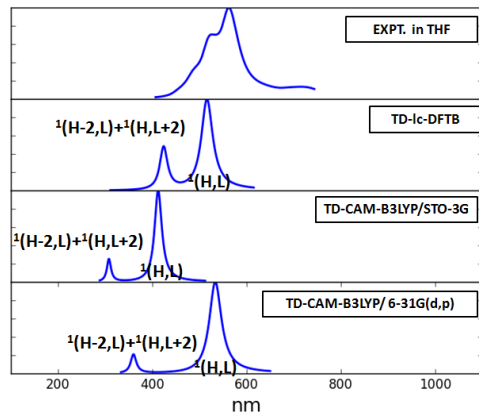


FIG. 18: Pentacene monomer absorption spectra: (a) TD-LDA, TD-DFTB, and experiment; (b) TD-B3LYP, TD-DFTB, and experiment; (c) TD-CAM-B3LYP, TD-lc-DFTB, and experiment. The experimental curve is a spectrum measured in tetrahydrofuran. Intensities are in arbitrary units.

TD-DFTB (and TD-lc-DFTB) calculations give qualitatively similar spectra in terms of the number and spacing of peaks, though not all peaks are shown in Fig. 18. Our concern is primarily with the lowest energy (i.e., longest wavelength) transitions.

Let us first look at the TD-DFT calculations with the 6-31G(d,p) basis set using different functionals. The TD-LDA/6-31G(d,p) spectrum is red-shifted with respect to the experimental spectrum. The TD-B3LYP/6-31G(d,p) spectrum, which includes some HF exchange via a global hybrid, brings us closer to the experimental spectrum. Finally the TD-CAM-B3LYP/6-31G(d,p) spectrum, which includes even more HF exchange to describe the long-range part of the electron-electron repulsion, matches the experimental spectrum very well. Of course, this should be taken with a certain amount of scepticism because the experimental spectrum is measured in solution while the theoretical calculations are for the gas phase and neglect any vibrational contributions.

Let us now turn to the TD-DFTB and TD-lc-DFTB calculations. Since these are semi-empirical calculations, they are expected to be similar to TD-DFT/STO-3G calculations in that DFTB calculations are parameterized assuming a minimal basis set. This might be expected to show up in the number of underlying degrees of freedom and hence in the complexity of the calculated absorption spectra. Indeed this does seem to be the case in that the longest wavelength TD-CAM-B3LYP/6-31G(d,p) peak shows more complexity than does the longest wavelength TD-lc-DFTB or TD-DFTB peak. (This difference is *not* visible in Fig. 18, but rather in the underlying stick spectra.) However the TD-lc-DFTB and TD-DFTB spectra are red-shifted compared to the correspondingly TD-DFT/STO-3G spectra. This brings the TD-DFTB spectrum in remarkably good correspondance with the TD-B3LYP/6-31G(d,p) spectrum and the TD-lc-DFTB spectrum in remarkably good correspondance with the TD-CAM-B3LYP/6-31G(d,p) spectrum.

Some rough assignments are given, based upon MO contributions to the TD-DFT and TD-DFTB (or TD-lc-DFTB) coefficients. The lowest energy peaks (Table II) are singlet HOMO \rightarrow LUMO transitions [$^1(H,L)$]. The $^1(H,L)$ TD-CAM-B3LYP/6-31G(d,p) peak is at 534 nm, which may be compared with the corresponding experimental value of about 540 nm from gas phase spectroscopy [122] and spectroscopy of isolated pentacene molecules in rare gas matrices [123]. The next lowest energy peaks have mixed $^1(H-2,L)$ and $^1(H,L+2)$ character as we have mentioned (Sec. II) often occurs in the

TABLE II: Monomer lowest energy peak $^1(H,L)$ calculated with various methods.

State	f (unitless)	λ (nm)	ΔE (eV)
Method			
TD-LDA/6-31G(d,p)//LDA/6-31G(d,p)			
$1^1 B_{1u}$	0.0234	744	1.67
TD-LDA/STO-3G//LDA/STO-3G			
$1^1 B_{1u}$	0.0325	579	2.14
TD-B3LYP/6-31G(d,p)//B3LYP/6-31G(d,p)			
$1^1 B_{1u}$	0.0415	633	1.96
TD-B3LYP/STO-3G//B3LYP/STO-3G			
$1^1 B_{1u}$	0.0596	492	2.52
TD-DFTB//DFTB			
$1^1 B_{1u}$	0.1594	646	1.92
TD-CAM-B3LYP/6-31G(d,p)//B3LYP/6-31G(d,p)			
$1^1 B_{1u}$	0.0750	534	2.32
TD-CAM-B3LYP/STO-3G//CAM-B3LYP/STO-3G			
$1^1 B_{1u}$	0.1070	412	3.01
TD-lc-DFTB//lc-DFTB			
$1^1 B_{1u}$	0.3212	515	2.40
HF/6-31G(d,p)//B3LYP/6-31G(d,p)			
$1^1 B_{1u}$	0.1436	491	2.53
HF/STO-3G//B3LYP/6-31G(d,p)			
$1^1 B_{1u}$	0.2279	357	3.47

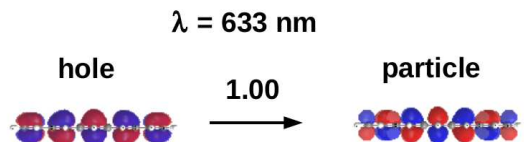


FIG. 19: Monomer NTOs and renormalized coefficient: TD-B3LYP/6-31G(d,p)//B3LYP/6-31G(d,p) 633 nm.

excitation spectra of π -conjugated molecules.

It is especially important to confirm our $^1(H,L)$ peak assignment. Figure 19 shows the natural transition orbitals (NTOs) associated with the lower energy peak in the spectrum. Comparison with the nodal structure in Figs. 16 and 17 confirms that this is indeed the $^1(H,L)$ transition.

Notice that there is a close analogy between the TOTEM model in ethylene and that of pentacene. In particular, the part of the H and L MOs on carbons 6 and 13 in pentacene (see Fig. 14) corresponds to a $\pi^* \rightarrow \pi$. This is sufficiently analogous to the $\pi \rightarrow \pi^*$ transition in ethylene that essentially the same theoretical analysis goes through for pentacene as for ethylene and we will make great use of this observation in the next subsection.

TABLE III: Intermolecular distances obtained for the tetramer of parallel stacked pentacene molecules.

Method	Distance (Å)
LDA/STO-3G	3.7
LDA/6-31G(d,p)	3.6
B3LYP+D3/STO-3G	3.5
B3LYP+D3/6-31G(d,p)	3.68
CAM-B3LYP+D3/STO-3G	3.5
CAM-B3LYP+D3/6-31G(d,p)	3.72
DFTB+D3	3.1
lc-DFTB+D3	3.1

B. Stacking

We are concerned with the model of equally-spaced stacked pentacenes shown in Fig. 15. This model, though far from the observed herringbone structure of solid pentacene, is interesting because of its obvious analogy to graphite and because it may be readily compared with the model of equally-spaced stacked ethylenes discussed in the previous section.

1. Intermolecular forces

Equally-spaced parallel stacked pentacenes were prepared by optimizing the intermolecular distance for stacked tetramers without reoptimizing the individual molecules. The tetramer stacked structure is expected to be bound together by van der Waals forces at a distance similar to that in graphene, namely about 3 Å [124].

Figure 20 shows the resultant PES for molecules without dispersion correction. As a general rule, DFT can only describe forces between atoms in regions of space where the electron density is significant. Uncorrected DFT is usually unable to describe van der Waals binding as such binding takes place at intermolecular distances where the molecular densities do not overlap significantly. As seen in Fig. 20, LDA/6-31G(d,p) shows an accidental minimum at about 3.65 Å but LDA/STO-3G does not bind. The other functionals do not bind whichever basis is used. DFTB also does not bind, but it is less repulsive than the other calculations shown here.

Figure 21 shows the improved curves obtained using Grimme’s D3 dispersion correction. The minima are located at at about 3.7 Å for B3LYP+D3, at about 3.72 Å for CAM-B3LYP+D3, and at about 3.1 Å for DFTB+D3.

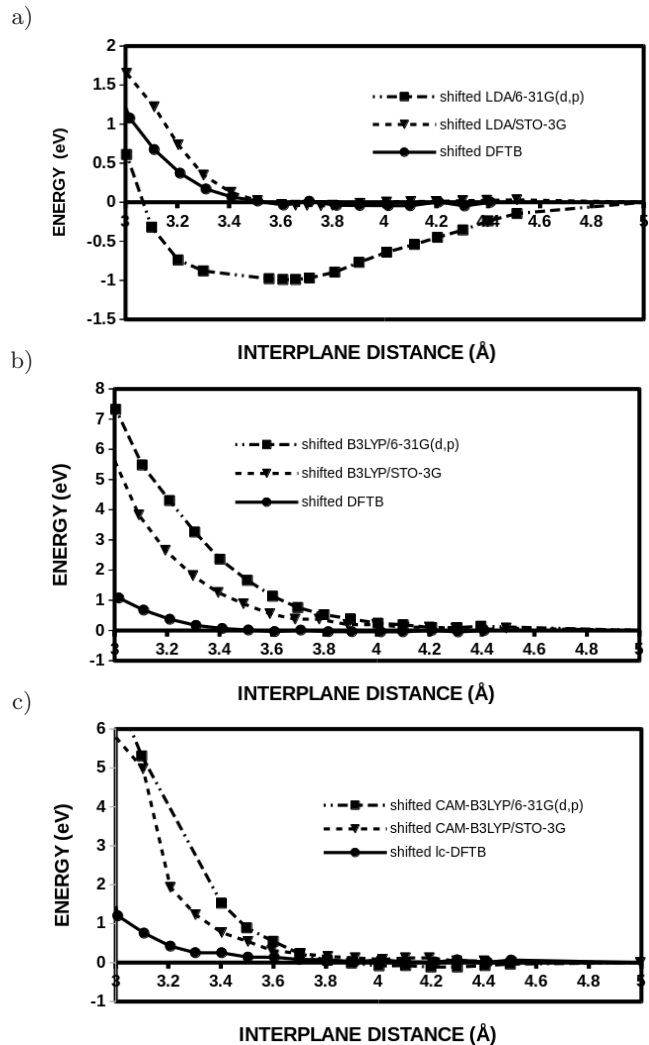


FIG. 20: Pentacene tetramer potential energy surfaces without dispersion correction: (a) LDA and DFTB; (b) B3LYP and DFTB; (c) CAM-B3LYP, lc-DFTB.

Optimized intermolecular distances are summarized in Table III.

2. Energy versus charge transfer

Now that we have determined an optimal stacking distance (namely 3.71 Å), we can use the analogy to stacked ethylenes developed in the previous section to estimate the relative contributions of CT versus ET in the ex-

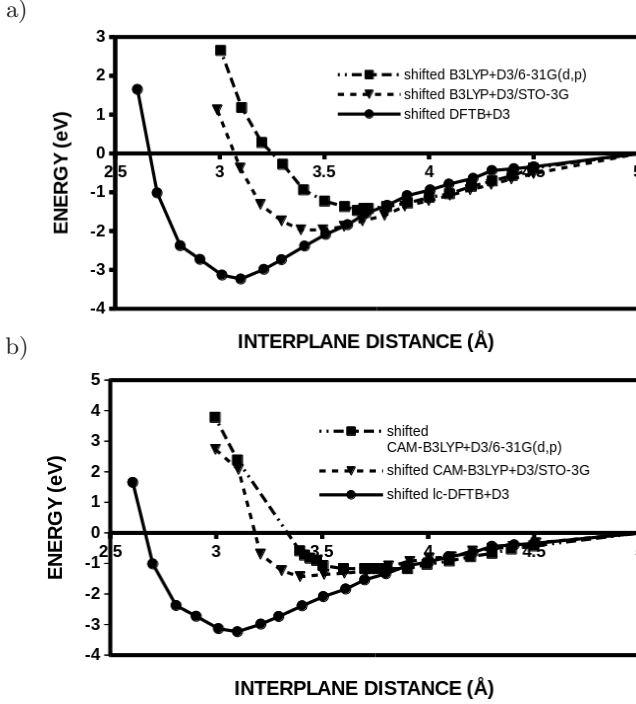


FIG. 21: Pentacene tetramer potential energy surfaces with dispersion correction: (a) B3LYP+D3 and DFTB+D3; (b) CAM-B3LYP+D3, lc-DFTB+D3.

citon model. This is possible by concentrating on the central part (carbons 6 and 13 of Fig. 14) of the $H(b_{2g})$ and $L(b_{3u})$ MOs in Fig. 16. This part of the pentacene $H(b_{2g})$ MO resembles the ethylene π^* MO while the pentacene $L(b_{3u})$ MO resembles the ethylene π MO (Fig. 2). Figure 19 shows a side view of the pentacene $H \rightarrow L$ transition. Looked at this way, the only important difference between the MOs for stacked pentacenes and the MOs for stacked ethylenes is that one MO diagram is the inverse of the other (i.e., bonding and antibonding orbitals have been interchanged).

Figure 22 shows the stacked pentacene dimer MOs which may be compared with the stacked ethylene dimer MOs (Fig. 4). It is easy to identify the coefficient c_1 for the ${}^1(H, L + 1)$ configuration and the coefficient c_2 for the ${}^1(H - 1, L)$ configuration. Table IV shows how the excitations split into a bright ET exciton and a much darker CT exciton. The energy splitting $DS = ET - CT$ is the Davydov splitting. Kasha's exciton model (Fig. 7) predicts a positive DS and this is exactly what is seen in our TD-LDA/6-

TABLE IV: Relative percentages of CT and ET excitonic transitions to the principle transition for two parallel stacked pentacenes as a function of method. See Eq. (2.5). DS is the Davydov splitting between the CT and ET excitonic transitions.

		Method			
State	f (unitless)	λ (nm)	ΔE (eV)	ET ^a	CT ^b
TD-LDA/6-31G(d,p)//LDA/6-31G(d,p)					
1^1B_{1u}	0.0002	1033	1.20	0.3%	99.9%
2^1B_{1u}	0.0322	733	1.69	99.9%	0.3%
DS ₂ = 0.49 eV					
TD-LDA/STO-3G//LDA/STO-3G					
1^1B_{1u}	0.0000	818	1.52	0.005%	99.9%
2^1B_{1u}	0.0499	572	2.17	99.9%	0.005%
DS ₂ = 0.65 eV					
TD-B3LYP/6-31G(d,p)//B3LYP+D3/6-31G(d,p)					
1^1B_{1u}	0.0005	735	1.69	2.9%	98.8%
2^1B_{1u}	0.0576	621	2.00	98.8%	2.9%
DS ₂ = 0.31 eV					
TD-B3LYP/STO-3G//B3LYP+D3/STO-3G					
1^1B_{1u}	0.0000	604	2.05	0.02%	100.0%
2^1B_{1u}	0.0897	484	2.56	99.9%	2.9%
DS ₂ = 0.51 eV					
TD-DFTB//DFTB+D3					
1^1B_{1u}	0.0001	872	1.42	0.05%	100.0%
2^1B_{1u}	0.2831	634	1.96	100.0%	0.06%
DS ₂ = 0.54 eV					
TD-CAM-B3LYP/6-31G(d,p)//B3LYP+D3/6-31G(d,p)					
1^1B_{1u}	0.1036	523	2.37	97.7%	3.0%
2^1B_{1u}	0.0033	489	2.54	3.0%	97.7%
DS ₂ = -0.17 eV					
TD-CAM-B3LYP/STO-3G//CAM-B3LYP+D3/STO-3G					
1^1B_{1u}	0.0004	423	2.93	0.2%	99.9%
2^1B_{1u}	0.1628	404	3.07	99.9%	0.2%
DS ₂ = 0.14 eV					
TD-lc-DFTB//lc-DFTB+D3					
1^1B_{1u}	0.5782	495	2.50	99.8%	0.24%
2^1B_{1u}	0.0013	451	2.75	0.21%	99.8%
DS ₂ = -0.25 eV					
TD-HF/6-31G(d,p)//B3LYP+D3/6-31G(d,p)					
1^1B_{1u}	0.2087	474	2.62	100.0%	0.07%
2^1B_{1u}	0.0002	332	3.73	0.06%	100.0%
DS ₂ = -1.11 eV					
TD-HF/STO-3G//B3LYP+D3/6-31G(d,p)					
1^1B_{1u}	0.3557	347	3.58	100.0%	0.01%
2^1B_{1u}	0.0001	282	4.40	0.01%	100.0%
DS ₂ = -0.82 eV					

$$^a (c_1 + c_2)^2 / 2.$$

$$^b (c_1 - c_2)^2 / 2.$$

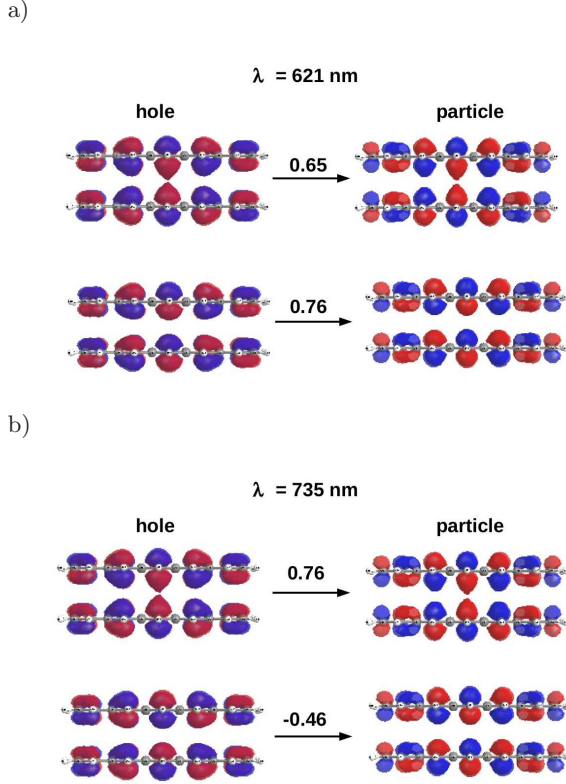


FIG. 22: Dimer NTOs and renormalized coefficients: (a) TD-B3LYP/6-31G(d,p)//D3-B3LYP/6-31G(d,p) 621 nm, (b) TD-B3LYP/6-31G(d,p)//D3-B3LYP/6-31G(d,p) 735 nm.

31G(d,p), TD-LDA/STO-3G, TD-B3LYP/6-31G(d,p), TD-B3LYP/STO-3G, TD-CAM-B3LYP/STO-3G, and TD-DFTB calculations. However, improving the description of charge transfer by adding more HF exchange leads to negative values of DS in the TD-CAM-B3LYP/6-31G(d,p), TD-HF/6-31G(d,p), TD-HF/STO-3G, and TD-*lc*-DFTB models and a very different picture of exciton coupling (Fig. 23). Careful rereading of the classic exciton theory article of Kasha, Rawls, and El-Bayoumi [8] reveals that they took into account only dipole-dipole interactions but not charge transfer effects. As these charge transfer effects are implicit in our calculations, we may explain the observation that Hartree-Fock exchange leads to CT excitonic states of higher energy than ET states by the large amount of energy needed to separate charges. Interestingly the DS obtained from

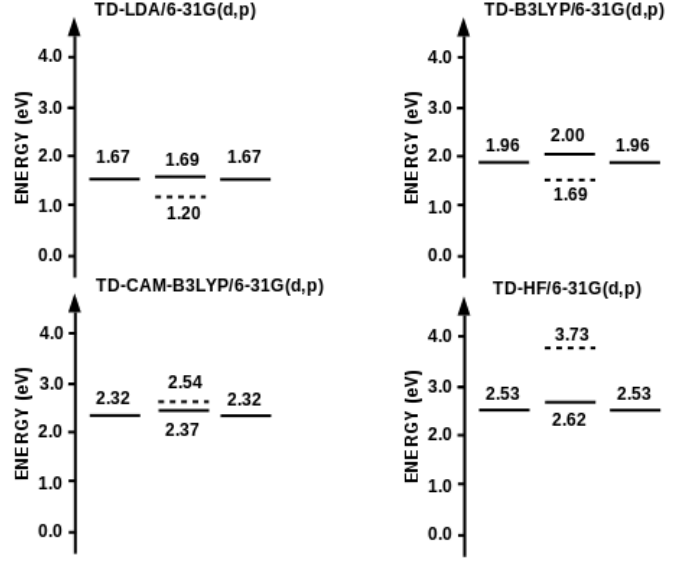


FIG. 23: Comparison of exciton diagrams for different functionals using the data from Tables II and IV.

TD-DFTB//D3-DFTB resembles most closely that obtained with the TD-B3LYP/STO-3G//D3-B3LYP/STO-3G or TD-LDA/STO-3G//D3-LDA/STO-3G, consistent with the idea that the DS is primarily determined by the overlap which is too small when a minimal basis set is used. The situation changes markedly in going to the long-range corrected functionals. Here the TD-*lc*-DFTB DS is closer to the TD-CAM-DFTB/6-31G(d,p) DS than to the TD-CAM-DFTB/STO-3G DS.

Tables V, VI, VII, VIII, and IX apply the analysis of Sec. II to the equally-spaced parallel stacked trimer. As expected, instead of a Davydov pair of ET and CT excitations, we find a Davydov triplet corresponding to the 2^1B_{1u} , 3^1B_{1u} , and 4^1B_{1u} states. When the Davydov pairs can be identified, we have highlighted their assignment in terms of nearest neighbor interactions in the tables. Cases where the Davydov pairs are clear are: TD-LDA/6-31G(d,p)//LDA/6-31G(d,p), TD-LDA/STO-3G//LDA/STO-3G, TD-B3LYP/6-31G(d,p)//B3LYP+D3/6-31G(d,p), TD-B3LYP/STO-3G//B3LYP+D3/STO-3G, TD-DFTB//DFTB+D3. In these cases, the (ET₁₂+ET₂₃)-dominated state is the highest energy transition of the Davydov triplet and also has the highest oscillator strength while the (CT₁₂+CT₂₃)-dominated state is the lowest energy transition of the Davydov triplet and has significantly

TABLE V: Relative percentages of CT and ET excitonic transitions to the principle transition for three parallel stacked pentacenes as a function of method. See Eq. (2.8). DS is the Davydov splitting between the lowest energy CT and the highest energy ET excitonic transitions.

State	f (unitless)	λ (nm)	Method	
			ΔE (eV)	
1^1B_{1u}	0.0000	2444	TD-LDA/6-31G(d,p)//LDA/6-31G(d,p)	
			0.51	
			Analysis	
			100%	$^1(H,L)$
			0% ^a	$(ET_{12}+ET_{23})/\sqrt{3}$
			0% ^b	$(\sqrt{3}/2)[ET_{13}-(1/3)(ET_{12}+ET_{23})]$
			0% ^c	$(CT_{12}+CT_{23})/\sqrt{2}$
			0% ^d	CT_{13}
			0%	$^1(H-2,L+2)$
			0%	1.20
2^1B_{1u}	0.0002	1040	Analysis	
			0%	$^1(H,L)$
			8.9% ^a	$(ET_{12}+ET_{23})/\sqrt{3}$
			2.9% ^b	$(\sqrt{3}/2)[ET_{13}-(1/3)(ET_{12}+ET_{23})]$
			81.9% ^c	$(CT_{12}+CT_{23})/\sqrt{2}$
			6.3% ^d	CT_{13}
			0%	$^1(H-2,L+2)$
			0%	1.30
			Analysis	
			0%	$^1(H,L)$
1.2% ^a	$(ET_{12}+ET_{23})/\sqrt{3}$			
34.2% ^b	$(\sqrt{3}/2)[ET_{13}-(1/3)(ET_{12}+ET_{23})]$			
7.6% ^c	$(CT_{12}+CT_{23})/\sqrt{2}$			
54.6% ^d	CT_{13}			
2.3%	$^1(H-2,L+2)$			
0%	1.70			
3^1B_{1u}	0.0003	950	Analysis	
			0%	$^1(H,L)$
			1.2% ^a	$(ET_{12}+ET_{23})/\sqrt{3}$
			34.2% ^b	$(\sqrt{3}/2)[ET_{13}-(1/3)(ET_{12}+ET_{23})]$
			7.6% ^c	$(CT_{12}+CT_{23})/\sqrt{2}$
			54.6% ^d	CT_{13}
			2.3%	$^1(H-2,L+2)$
			0%	1.70
			Analysis	
			0%	$^1(H,L)$
80.6% ^a	$(ET_{12}+ET_{23})/\sqrt{3}$			
19.1% ^b	$(\sqrt{3}/2)[ET_{13}-(1/3)(ET_{12}+ET_{23})]$			
0.3% ^c	$(CT_{12}+CT_{23})/\sqrt{2}$			
0.02% ^d	CT_{13}			
0%	$^1(H-2,L+2)$			
DS ₃ = 0.50 eV				
1^1B_{1u}	0.0000	1024	TD-LDA/STO-3G//LDA/STO-3G	
			1.21	
			Analysis	
			88.4%	$^1(H,L)$
			0.1% ^a	$(ET_{12}+ET_{23})/\sqrt{3}$
			3.5% ^b	$(\sqrt{3}/2)[ET_{13}-(1/3)(ET_{12}+ET_{23})]$
			2.3% ^c	$(CT_{12}+CT_{23})/\sqrt{2}$
			5.7% ^d	CT_{13}
			0%	$^1(H-2,L+2)$
			0%	1.52
2^1B_{1u}	0.0000	816	Analysis	
			0%	$^1(H,L)$
			0.3% ^a	$(ET_{12}+ET_{23})/\sqrt{3}$
			7.3% ^b	$(\sqrt{3}/2)[ET_{13}-(1/3)(ET_{12}+ET_{23})]$
			79.7% ^c	$(CT_{12}+CT_{23})/\sqrt{2}$
			12.7% ^d	CT_{13}
			0%	$^1(H-2,L+2)$
			0%	1.64
			Analysis	
			7.2%	$^1(H,L)$
0.1% ^a	$(ET_{12}+ET_{23})/\sqrt{3}$			
39.2% ^b	$(\sqrt{3}/2)[ET_{13}-(1/3)(ET_{12}+ET_{23})]$			
0%	$^1(H-2,L+2)$			
0%	2.30			
3^1B_{1u}	0.0000	754	Analysis	
			7.2%	$^1(H,L)$
			0.1% ^a	$(ET_{12}+ET_{23})/\sqrt{3}$
			39.2% ^b	$(\sqrt{3}/2)[ET_{13}-(1/3)(ET_{12}+ET_{23})]$
			0%	$^1(H-2,L+2)$
			0%	2.30

TABLE VI: Relative percentages of CT and ET excitonic transitions to the principle transition for three parallel stacked pentacenes as a function of method. See Eq. (2.8). DS is the Davydov splitting between the lowest energy CT and the highest energy ET excitonic transitions.

State	f (unitless)	λ (nm)	Method	
			ΔE (eV)	
1^1B_{1u}	0.0001	1220	TD-B3LYP/6-31G(d,p)//B3LYP+D3/6-31G(d,p)	
			1.02	
			Analysis	
			100.0%	$^1(H,L)$
			0% ^a	$(ET_{12}+ET_{23})/\sqrt{3}$
			0% ^b	$(\sqrt{3}/2)[ET_{13}-(1/3)(ET_{12}+ET_{23})]$
			0% ^c	$(CT_{12}+CT_{23})/\sqrt{2}$
			0% ^d	CT_{13}
			0%	$^1(H-2,L+2)$
			0%	1.69
2^1B_{1u}	0.0006	734	Analysis	
			0%	$^1(H,L)$
			0.8% ^a	$(ET_{12}+ET_{23})/\sqrt{3}$
			0% ^b	$(\sqrt{3}/2)[ET_{13}-(1/3)(ET_{12}+ET_{23})]$
			98.8% ^c	$(CT_{12}+CT_{23})/\sqrt{2}$
			0.3% ^d	CT_{13}
			0%	$^1(H-2,L+2)$
			0%	1.89
			Analysis	
			0%	$^1(H,L)$
0.6% ^a	$(ET_{12}+ET_{23})/\sqrt{3}$			
39.7% ^b	$(\sqrt{3}/2)[ET_{13}-(1/3)(ET_{12}+ET_{23})]$			
0.2% ^c	$(CT_{12}+CT_{23})/\sqrt{2}$			
59.5% ^d	CT_{13}			
0%	$^1(H-2,L+2)$			
0%	2.01			
3^1B_{1u}	0.0012	657	Analysis	
			0%	$^1(H,L)$
			0.6% ^a	$(ET_{12}+ET_{23})/\sqrt{3}$
			39.7% ^b	$(\sqrt{3}/2)[ET_{13}-(1/3)(ET_{12}+ET_{23})]$
			0.2% ^c	$(CT_{12}+CT_{23})/\sqrt{2}$
			59.5% ^d	CT_{13}
			0%	$^1(H-2,L+2)$
			0%	1.89
			Analysis	
			0%	$^1(H,L)$
0.6% ^a	$(ET_{12}+ET_{23})/\sqrt{3}$			
39.7% ^b	$(\sqrt{3}/2)[ET_{13}-(1/3)(ET_{12}+ET_{23})]$			
0.2% ^c	$(CT_{12}+CT_{23})/\sqrt{2}$			
59.5% ^d	CT_{13}			
0%	$^1(H-2,L+2)$			
0%	2.01			
4^1B_{1u}	0.0723	618	Analysis	
			0%	$^1(H,L)$
			82.9% ^a	$(ET_{12}+ET_{23})/\sqrt{3}$
			15.8% ^b	$(\sqrt{3}/2)[ET_{13}-(1/3)(ET_{12}+ET_{23})]$
			0.9% ^c	$(CT_{12}+CT_{23})/\sqrt{2}$
			0.4% ^d	CT_{13}
			0%	$^1(H-2,L+2)$
			0%	2.01
			Analysis	
			0%	$^1(H,L)$
82.9% ^a	$(ET_{12}+ET_{23})/\sqrt{3}$			
15.8% ^b	$(\sqrt{3}/2)[ET_{13}-(1/3)(ET_{12}+ET_{23})]$			
0.9% ^c	$(CT_{12}+CT_{23})/\sqrt{2}$			
0.4% ^d	CT_{13}			
0%	$^1(H-2,L+2)$			
DS ₃ = 0.32 eV				
1^1B_{1u}	0.0001	801	TD-B3LYP/STO-3G//B3LYP+D3/STO-3G	
			1.55	
			Analysis	
			100%	$^1(H,L)$
			0% ^a	$(ET_{12}+ET_{23})/\sqrt{3}$
			0% ^b	$(\sqrt{3}/2)[ET_{13}-(1/3)(ET_{12}+ET_{23})]$
			0% ^c	$(CT_{12}+CT_{23})/\sqrt{2}$
			0% ^d	CT_{13}
			0%	$^1(H-2,L+2)$
			0%	2.06
2^1B_{1u}	0.0000	602	Analysis	
			0%	$^1(H,L)$
			0.0% ^a	$(ET_{12}+ET_{23})/\sqrt{3}$
			0% ^b	$(\sqrt{3}/2)[ET_{13}-(1/3)(ET_{12}+ET_{23})]$
			100.0% ^c	$(CT_{12}+CT_{23})/\sqrt{2}$
			0.0% ^d	CT_{13}
			0%	$^1(H-2,L+2)$
			0%	2.30
			Analysis	
			0%	$^1(H,L)$
7.0% ^a	$(ET_{12}+ET_{23})/\sqrt{3}$			
79.6% ^b	$(\sqrt{3}/2)[ET_{13}-(1/3)(ET_{12}+ET_{23})]$			
0%	$^1(H-2,L+2)$			
0%	2.30			
3^1B_{1u}	0.0003	539	Analysis	
			0%	$^1(H,L)$
			7.0% ^a	$(ET_{12}+ET_{23})/\sqrt{3}$
			79.6% ^b	$(\sqrt{3}/2)[ET_{13}-(1/3)(ET_{12}+ET_{23})]$
			0%	$^1(H-2,L+2)$
			0%	2.30

TABLE VII: Relative percentages of CT and ET excitonic transitions to the principle transition for three parallel stacked pentacenes as a function of method. See Eq. (2.8). DS is the Davydov splitting between the lowest energy CT and the highest energy ET excitonic transitions.

State	f (unitless)	λ (nm)	Method	ΔE (eV)
1^1B_{1u}	0.0000	1606	TD-DFTB//DFTB+D3	0.772
			Analysis	
			86.9%	$^1(H,L)$
			1.6% ^a	$(ET_{12}+ET_{23})/\sqrt{3}$
			6.6% ^b	$(\sqrt{3}/2)[ET_{13}-(1/3)(ET_{12}+ET_{23})]$
0% ^c	$(CT_{12}+CT_{23})/\sqrt{2}$			
4.9% ^d	CT_{13}			
0%	$^1(H-2,L+2)$			
2^1B_{1u}	0.0002	872	TD-DFTB//DFTB+D3	1.42
			Analysis	
			0%	$^1(H,L)$
			0.01% ^a	$(ET_{12}+ET_{23})/\sqrt{3}$
			0% ^b	$(\sqrt{3}/2)[ET_{13}-(1/3)(ET_{12}+ET_{23})]$
99.9% ^c	$(CT_{12}+CT_{23})/\sqrt{2}$			
0.03% ^d	CT_{13}			
0%	$^1(H-2,L+2)$			
3^1B_{1u}	0.0004	819	TD-DFTB//DFTB+D3	1.51
			Analysis	
			0%	$^1(H,L)$
			6.0% ^a	$(ET_{12}+ET_{23})/\sqrt{3}$
			39.8% ^b	$(\sqrt{3}/2)[ET_{13}-(1/3)(ET_{12}+ET_{23})]$
7.5% ^c	$(CT_{12}+CT_{23})/\sqrt{2}$			
46.7% ^d	CT_{13}			
0%	$^1(H-2,L+2)$			
4^1B_{1u}	0.4122	624	TD-DFTB//DFTB+D3	1.99
			Analysis	
			0%	$^1(H,L)$
			4.2% ^a	$(ET_{12}+ET_{23})/\sqrt{3}$
			47.6% ^b	$(\sqrt{3}/2)[ET_{13}-(1/3)(ET_{12}+ET_{23})]$
40.3% ^c	$(CT_{12}+CT_{23})/\sqrt{2}$			
7.9% ^d	CT_{13}			
0%	$^1(H-2,L+2)$			
DS ₃ = 0.57 eV				

TABLE VIII: Relative percentages of CT and ET excitonic transitions to the principle transition for three parallel stacked pentacenes as a function of method. See Eq. (2.8). DS is the Davydov splitting between the lowest energy CT and the highest energy ET excitonic transitions.

State	f (unitless)	λ (nm)	Method	ΔE (eV)
1^1B_{1u}	0.0006	544	TD-CAM-B3LYP/STO-3G//CAM-B3LYP+D3/STO-3G	2.28
			Analysis	
			93.0%	$^1(H,L)$
			4.1% ^a	$(ET_{12}+ET_{23})/\sqrt{3}$
			1.7% ^b	$(\sqrt{3}/2)[ET_{13}-(1/3)(ET_{12}+ET_{23})]$
0% ^c	$(CT_{12}+CT_{23})/\sqrt{2}$			
1.2% ^d	CT_{13}			
0%	$^1(H-2,L+2)$			
2^1B_{1u}	0.0000	423	TD-CAM-B3LYP/STO-3G//CAM-B3LYP+D3/STO-3G	2.93
			Analysis	
			0%	$^1(H,L)$
			4.4% ^a	$(ET_{12}+ET_{23})/\sqrt{3}$
			0% ^b	$(\sqrt{3}/2)[ET_{13}-(1/3)(ET_{12}+ET_{23})]$
89.7% ^c	$(CT_{12}+CT_{23})/\sqrt{2}$			
5.9% ^d	CT_{13}			
0%	$^1(H-2,L+2)$			
3^1B_{1u}	0.2165	402	TD-CAM-B3LYP/STO-3G//CAM-B3LYP+D3/STO-3G	3.08
			Analysis	
			0%	$^1(H,L)$
			79.6% ^a	$(ET_{12}+ET_{23})/\sqrt{3}$
			20.3% ^b	$(\sqrt{3}/2)[ET_{13}-(1/3)(ET_{12}+ET_{23})]$
0.03% ^c	$(CT_{12}+CT_{23})/\sqrt{2}$			
0.1% ^d	CT_{13}			
0%	$^1(H-2,L+2)$			
4^1B_{1u}	0.0001	371	TD-CAM-B3LYP/STO-3G//CAM-B3LYP+D3/STO-3G	3.34
			Analysis	
			0%	$^1(H,L)$
			3.4% ^a	$(ET_{12}+ET_{23})/\sqrt{3}$
			23.9% ^b	$(\sqrt{3}/2)[ET_{13}-(1/3)(ET_{12}+ET_{23})]$
0.7% ^c	$(CT_{12}+CT_{23})/\sqrt{2}$			
45.1% ^d	CT_{13}			
26.8%	$^1(H-2,L+2)$			
DS ₃ = 0.15 eV				

State	f (unitless)	λ (nm)	Method	ΔE (eV)
1^1B_{1u}	0.0005	764	TD-CAM-B3LYP/6-31G(d,p)//B3LYP+D3/6-31G(d,p)	1.62
			Analysis	
			94.5%	$^1(H,L)$
			0.7% ^a	$(ET_{12}+ET_{23})/\sqrt{3}$
			2.7% ^b	$(\sqrt{3}/2)[ET_{13}-(1/3)(ET_{12}+ET_{23})]$
0% ^c	$(CT_{12}+CT_{23})/\sqrt{2}$			
2.0% ^d	CT_{13}			
0%	$^1(H-2,L+2)$			
2^1B_{1u}	0.1301	520	TD-CAM-B3LYP/6-31G(d,p)//B3LYP+D3/6-31G(d,p)	2.38
			Analysis	
			0%	$^1(H,L)$
			74.4% ^a	$(ET_{12}+ET_{23})/\sqrt{3}$
			20.6% ^b	$(\sqrt{3}/2)[ET_{13}-(1/3)(ET_{12}+ET_{23})]$
4.9% ^c	$(CT_{12}+CT_{23})/\sqrt{2}$			
0.06% ^d	CT_{13}			
0%	$^1(H-2,L+2)$			
3^1B_{1u}	0.0074	489	TD-CAM-B3LYP/6-31G(d,p)//B3LYP+D3/6-31G(d,p)	2.53
			Analysis	
			0%	$^1(H,L)$
			4.5% ^a	$(ET_{12}+ET_{23})/\sqrt{3}$
			0% ^b	$(\sqrt{3}/2)[ET_{13}-(1/3)(ET_{12}+ET_{23})]$

State	f (unitless)	λ (nm)	Method	ΔE (eV)
1^1B_{1u}	0.0028	705	TD-lc-DFTB//lc-DFTB+D3	1.76
			Analysis	
			88.4%	$^1(H,L)$
			1.5% ^a	$(ET_{12}+ET_{23})/\sqrt{3}$
			5.8% ^b	$(\sqrt{3}/2)[ET_{13}-(1/3)(ET_{12}+ET_{23})]$
0% ^c	$(CT_{12}+CT_{23})/\sqrt{2}$			
4.4% ^d	CT_{13}			
0%	$^1(H-2,L+2)$			
2^1B_{1u}	0.8238	487	TD-lc-DFTB//lc-DFTB+D3	2.54
			Analysis	
			0%	$^1(H,L)$
			29.6% ^a	$(ET_{12}+ET_{23})/\sqrt{3}$
			26.0% ^b	$(\sqrt{3}/2)[ET_{13}-(1/3)(ET_{12}+ET_{23})]$
14.2% ^c	$(CT_{12}+CT_{23})/\sqrt{2}$			
30.2% ^d	CT_{13}			
0%	$^1(H-2,L+2)$			
3^1B_{1u}	0.0018	452	TD-lc-DFTB//lc-DFTB+D3	2.74
			Analysis	
			0%	$^1(H,L)$
			0.01% ^a	$(ET_{12}+ET_{23})/\sqrt{3}$
			0% ^b	$(\sqrt{3}/2)[ET_{13}-(1/3)(ET_{12}+ET_{23})]$

TABLE IX: Relative percentages of CT and ET excitonic transitions to the principle transition for three parallel stacked pentacenes as a function of method. See Eq. (2.8). DS is the Davydov splitting between the lowest energy CT and the highest energy ET excitonic transitions.

		Method		
State	f (unitless)	λ (nm)	ΔE (eV)	
1^1B_{1u}	0.0051	417	TD-HF/STO-3G//B3LYP+D3/6-31G(d,p)	
			2.97	
	Analysis			

	$1^1(H,L)$			
	77.8%			
	$(\mathbf{ET}_{12}+\mathbf{ET}_{23})/\sqrt{3}$			
	0.2% ^a			
	$(\sqrt{3}/2)[\mathbf{ET}_{13}-(1/3)(\mathbf{ET}_{12}+\mathbf{ET}_{23})]$			
	8.4% ^b			
$(\mathbf{CT}_{12}+\mathbf{CT}_{23})/\sqrt{2}$				
1.4% ^c				
\mathbf{CT}_{13}				
9.6% ^d				
$1^1(H-2,L+2)$				
6.9%				
2^1B_{1u}	0.4703	343	3.62	
			Analysis	

	$1^1(H,L)$			
	0%			
	$(\mathbf{ET}_{12}+\mathbf{ET}_{23})/\sqrt{3}$			
	89.4% ^a			
	$(\sqrt{3}/2)[\mathbf{ET}_{13}-(1/3)(\mathbf{ET}_{12}+\mathbf{ET}_{23})]$			
	21.2% ^b			
	$(\mathbf{CT}_{12}+\mathbf{CT}_{23})/\sqrt{2}$			
0.02% ^c				
\mathbf{CT}_{13}				
0.02% ^d				
$1^1(H-2,L+2)$				
0%				
3^1B_{1u}	0.0001	283	4.38	
			Analysis	

	$1^1(H,L)$			
	4.3%			
	$(\mathbf{ET}_{12}+\mathbf{ET}_{23})/\sqrt{3}$			
	0.65% ^a			
	$(\sqrt{3}/2)[\mathbf{ET}_{13}-(1/3)(\mathbf{ET}_{12}+\mathbf{ET}_{23})]$			
	0%			
	$(\mathbf{CT}_{12}+\mathbf{CT}_{23})/\sqrt{2}$			
91.1% ^c				
\mathbf{CT}_{13}				
0.22% ^d				
$1^1(H-2,L+2)$				
3.7%				
4^1B_{1u}	0.0000	270	4.59	
			Analysis	

	$1^1(H,L)$			
	18.3%			
	$(\mathbf{ET}_{12}+\mathbf{ET}_{23})/\sqrt{3}$			
	1.3% ^a			
	$(\sqrt{3}/2)[\mathbf{ET}_{13}-(1/3)(\mathbf{ET}_{12}+\mathbf{ET}_{23})]$			
	9.5% ^b			
	$(\mathbf{CT}_{12}+\mathbf{CT}_{23})/\sqrt{2}$			
9.5% ^c				
\mathbf{CT}_{13}				
17.8% ^d				
$1^1(H-2,L+2)$				
48.4%				
$\mathbf{DS}_3 = -1.06$ eV				
1^1B_{1u}	0.0025	662	1.87	
			Analysis	

	$1^1(H,L)$			
	81.0%			
	$(\mathbf{ET}_{12}+\mathbf{ET}_{23})/\sqrt{3}$			
	0.2% ^a			
	$(\sqrt{3}/2)[\mathbf{ET}_{13}-(1/3)(\mathbf{ET}_{12}+\mathbf{ET}_{23})]$			
	7.1% ^b			
	$(\mathbf{CT}_{12}+\mathbf{CT}_{23})/\sqrt{2}$			
3.1% ^c				
\mathbf{CT}_{13}				
13.9% ^d				
$1^1(H-2,L+2)$				
0%				
2^1B_{1u}	0.2682	468	2.65	
			Analysis	

	$1^1(H,L)$			
	0%			
	$(\mathbf{ET}_{12}+\mathbf{ET}_{23})/\sqrt{3}$			
	89.0% ^a			
	$(\sqrt{3}/2)[\mathbf{ET}_{13}-(1/3)(\mathbf{ET}_{12}+\mathbf{ET}_{23})]$			
	21.8% ^b			
	$(\mathbf{CT}_{12}+\mathbf{CT}_{23})/\sqrt{2}$			
0.11% ^c				
\mathbf{CT}_{13}				
0.003% ^d				
$1^1(H-2,L+2)$				
0%				
3^1B_{1u}	0.0002	334	3.71	
			Analysis	

	$1^1(H,L)$			
	4.0%			
	$(\mathbf{ET}_{12}+\mathbf{ET}_{23})/\sqrt{3}$			
	1.5% ^a			
	$(\sqrt{3}/2)[\mathbf{ET}_{13}-(1/3)(\mathbf{ET}_{12}+\mathbf{ET}_{23})]$			
	0%			

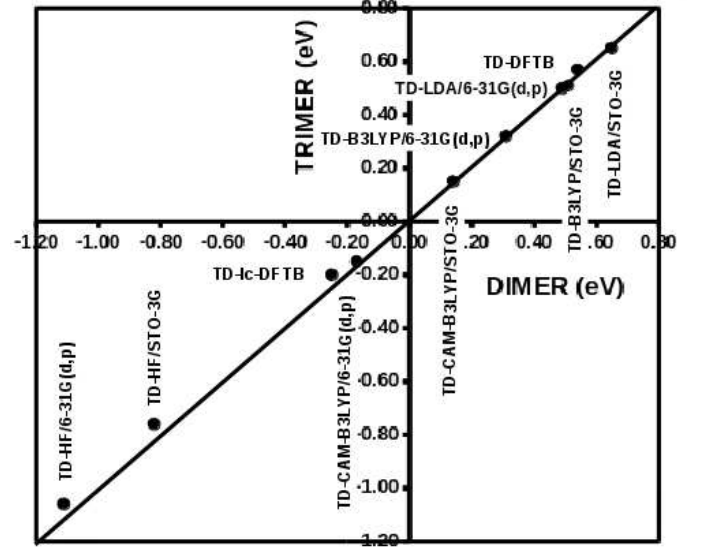


FIG. 24: Graph comparing the Davydov splittings, $E(\mathbf{ET})-E(\mathbf{CT})$, of the trimer and dimer. The 45° line indicates perfect agreement between dimer and trimer Davydov splittings.

less oscillator strength. A third contribution to the Davydov triplet lies between the two other states and also has only a feeble transition energy. This assignment is a bit less clear in the TD-DFTB//DFTB+D3 case because there is significant mixing between $\mathbf{ET}_{12}+\mathbf{ET}_{23}$ and \mathbf{ET}_{13} in the brightest configuration. Henceforth we shall simply assume that the peak with the highest oscillator strength is an $(\mathbf{ET}_{12}+\mathbf{ET}_{23})$ -dominated state. Figure 24 shows that calculations with these methods give essentially the same Davydov splitting for the dimer and for the trimer, and that the dimer (\mathbf{DS}_2) and trimer (\mathbf{DS}_3) splittings are very similar for TD-DFTB and for TD-B3LYP/6-31G(d,p), as well as being very similar for TD-lc-DFT and for TD-CAM-B3LYP/6-31G(d,p).

3. Spectra

Calculations beyond the trimer become increasingly complicated to analyze but we may compare calculated spectra for increasingly large numbers of parallel stacked pentacene molecules. The tight-binding calculation in Sec. II is based upon the hope that nearest neighbor interactions dominate excitonic effects in spectra. The comparison of dimer and trimer DSs seem to at least partially confirm this. We may make a further check by

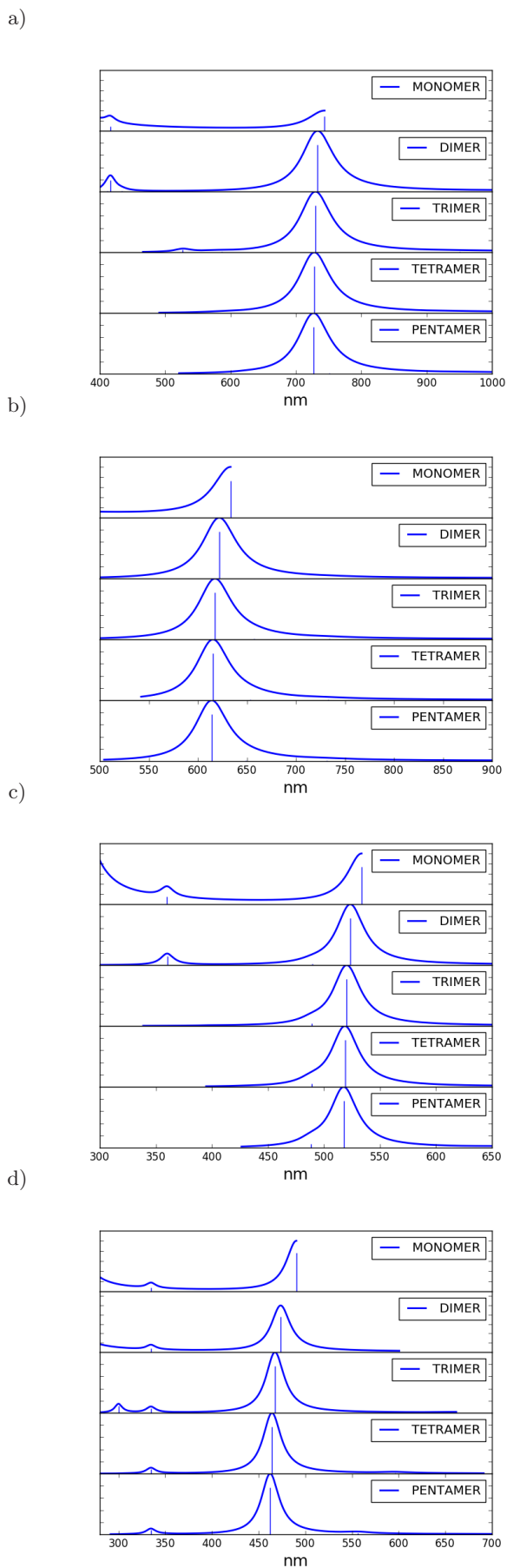


FIG. 25: Convergence of spectra as a function of

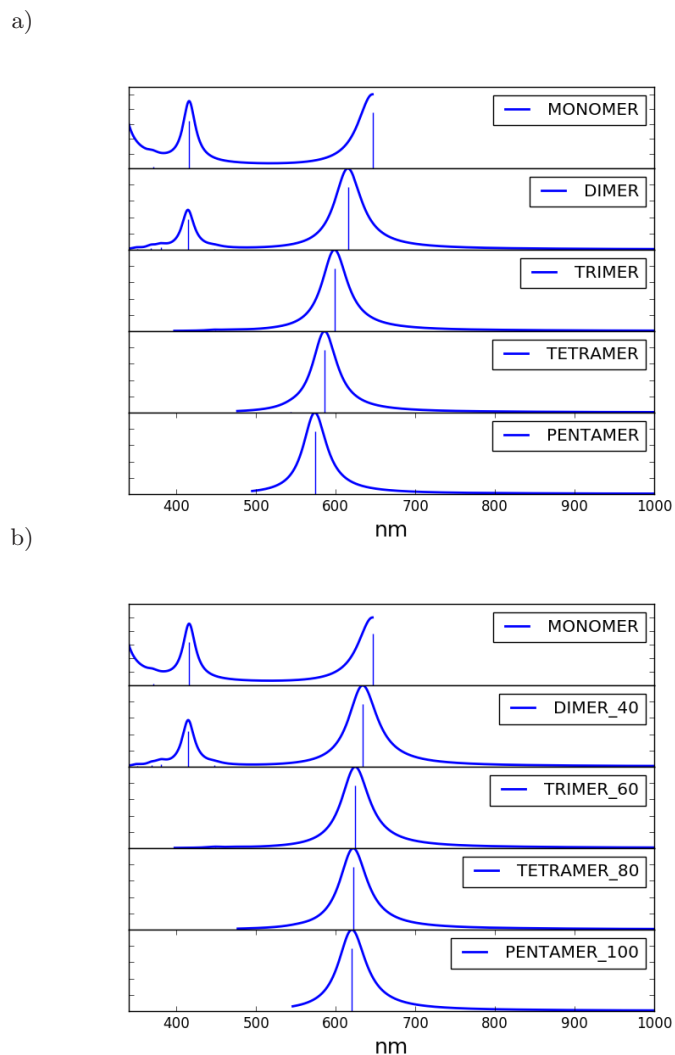
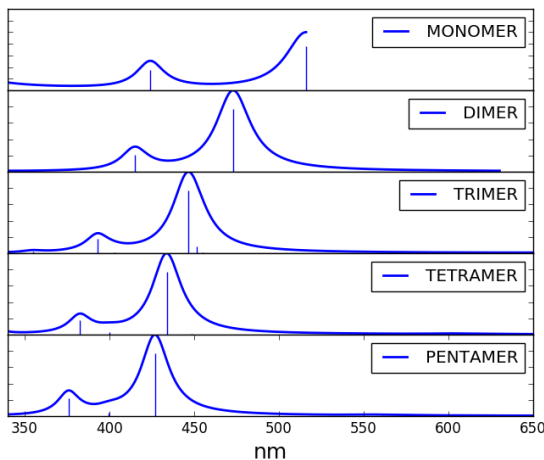


FIG. 26: TD-DFTB spectra of stacked pentacene: (a) with a fixed active space, (b) with a size-extensive active space.

seeing how the spectra change as more and more pentacene molecules are stacked. These spectra are shown in Fig. 25. All of the spectra show a main peak (i.e., the ET peak) which blue shifts as the pentacene stack grows. More specifically, the graphs show a main peak which undergoes the largest shift in going from the monomer to the dimer, a smaller shift in going from the dimer to the trimer and then shifts very little in going to higher oligomers, consistent with the suppositions behind the tight-binding model.

Our TD-DFT and TD-*lc*-DFTB calculations led us to

a)



b)

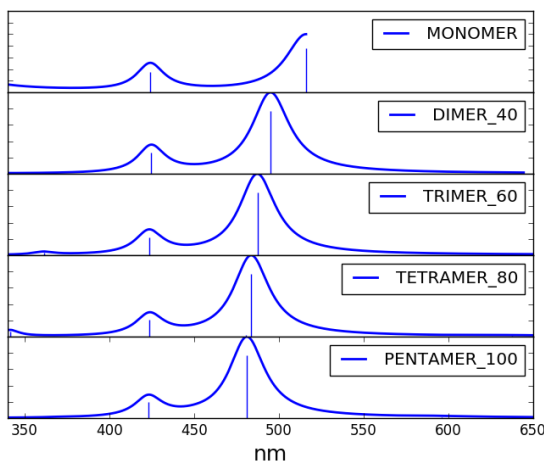


FIG. 27: TD-ic-DFTB spectra of stacked pentacene: (a) with a fixed active space, (b) with a size-consistent active space.

become aware of a problem already reported in Ref. 104. It is in the spirit of semi-empirical approaches to make simplifying approximations which allow the treatment of larger molecules than would otherwise be possible. This is why DFTBABY restricts the space of active orbitals, but it is still up to the user to decide how to use this option. One way would be to increase the size of the active space until converged spectra are achieved. But this ideal approach is not really practical when going to larger and larger aggregates of molecules. Instead, the first idea that comes to mind is to use the largest active space for

which calculations are possible. In practice, this means using the same number of occupied and unoccupied orbitals in the active space, independent of the number of molecules. We call doing this a calculation with a *fixed active space*. However it has the important drawback when describing size-dependent trends that fixed active space calculations have more basis functions per molecule for smaller aggregates than for larger aggregates and so invariably describe smaller aggregates better than larger aggregates with the introduction of corresponding systematic errors in the resultant size-dependent properties. The other approach is to keep the number of occupied and unoccupied orbitals in the active space proportional to the number of molecules. In this way, we hope to obtain a better description of size-dependent trends, albeit at some cost of accuracy for smaller aggregates. We call this doing a calculation with a *size-consistent active space*. (There is some confusion in the literature between the terms “size-consistent” and “size-extensive.” Both terms are arguably correct here, but we shall stick to “size-consistent.”) Figures 26 and 27 compare fixed and size-consistent active space calculations. The fixed active space calculations use 20 occupied orbitals and 20 unoccupied orbitals per aggregate. The size-consistent active space calculations use 20 occupied and 20 unoccupied orbitals per pentacene molecule. As the figure shows, the calculations with fixed active space blue shifts much more than do the calculations with self-consistent active space as the number of pentacene molecules increases. TD-DFT calculations of excitation energies are variational in the Tamm-Dancoff approximation and pseudo-variational in the sense that full linear response calculations often give similar results to using the Tamm-Dancoff approximation. For the monomer the fixed active space and size-consistent active space calculations are identical; however for the aggregates, the size-consistent active space is larger than the fixed active space calculations, leading to lower excitation energies in the size-consistent active space calculations. One would hope that the larger basis set would give better and answers and that this is the case is shown in Fig. 28 where it is seen that TD-DFTB and TD-B3LYP/6-31G(d,p) spectral peak locations differ by only about 10 nm. Figure 26 shows that the difference between the TD-DFTB and TD-B3LYP/6-31G(d,p) calculations would have been more like 50 nm had the fixed active space been used. Figure 28 also shows that the differences between TD-ic-DFTB and TD-CAM-B3LYP/6-31G(d,p) spectra are larger than for the TD-DFTB and TD-B3LYP/6-31G(d,p) case when the size-extensive active space is

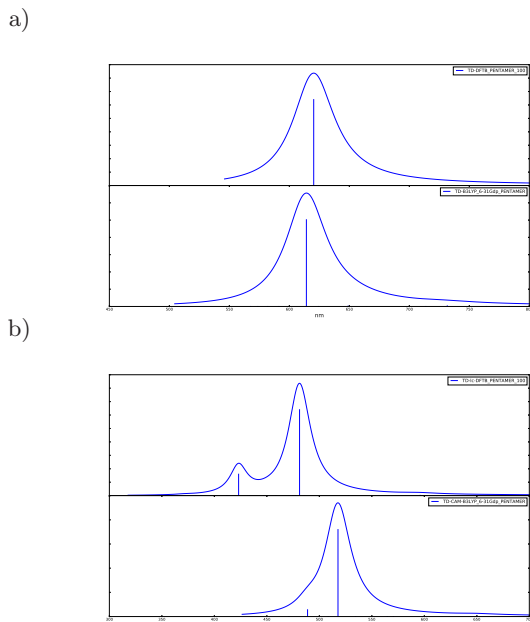


FIG. 28: Comparison of pentacene spectra: (a) TD-DFTB and TD-B3LYP/6-31G(d,p) and (b) TD-lc-DFTB and TD-CAM-B3LYP/6-31G(d,p).

used, with the main peak in this part of the spectrum having an energy difference of around 30 nm between the two calculations. Interestingly both show qualitatively similar Davydov multiplets. Figure 27 shows that the difference between the TD-lc-DFTB and TD-CAM-B3LYP(d,p) calculations would have been more like 80 nm had the fixed active space been used. This is why, except for Figs. 26 and 27, we have been careful to use a size-consistent active space consisting of 20 occupied and 20 unoccupied orbitals per molecule in all the TD-DFTB and TD-lc-DFTB reported in this paper.

C. Herringbone

The main objective of the present work has been to evaluate the ability of TD-DFTB and TD-lc-DFTB to simulate, respectively, the results of TD-B3LYP/6-31G(d,p) and TD-CAM-B3LYP/6-31G(d,p) calculations. While this has been largely satisfied by our study of parallel stacked pentacene molecules, the case of parallel stacked molecules is too artificial to allow comparison against experiment (except for the monomer.)

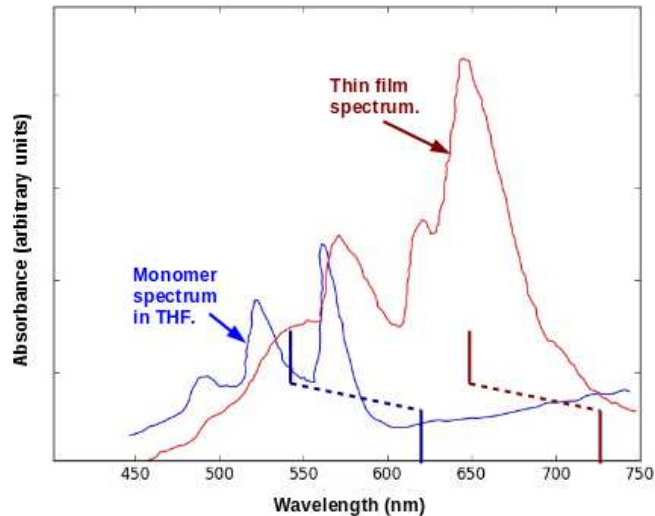


FIG. 29: Excitonic effects on the absorption spectrum of pentacene: curves, pentacene in tetrahydrofuran (THF) and as a thin film (from Ref. 121); stick spectra, lower are the position of unshifted monomer and crystal peaks calculated using the Bethe-Salpeter equation (BSE) while the upper stick spectra have been shifted to match the experiment (from Ref. 20.) See also Ref. 125.

In order to have a reality check, we have also carried out calculations for cluster models of pentacene crystals. The experimental spectrum of the molecule and of the crystal are available both from experiment [121, 126, 127] and from state-of-the-art theoretical calculations [20, 125, 128–130]. These are shown in Fig. 29. This time excitonic shifts lead to a red shift, rather than a blue shift. The structure of the spectrum suggests that both CT and ET transitions contribute to the spectrum. As we shall see, charge transfer is more important for describing excitonic effects in the absorption spectrum than is the case for parallel stacked pentamers.

We carried out calculations for the cluster models shown in Fig. 30 obtained by cutting out different portions of the x-ray crystal structure [117, 118] without any subsequent relaxation. Unless otherwise indicated all of the results reported below are for the “horizontal” decamer model. The picture of the horizontal model makes it clear that the crystal is made up of layers of tilted stacks of pentamers whose tilt angles alternate from layer to layer to provide a herringbone structure.

Figure 31 shows the herringbone spectra calculated at various levels and compared with the thin film spectrum.

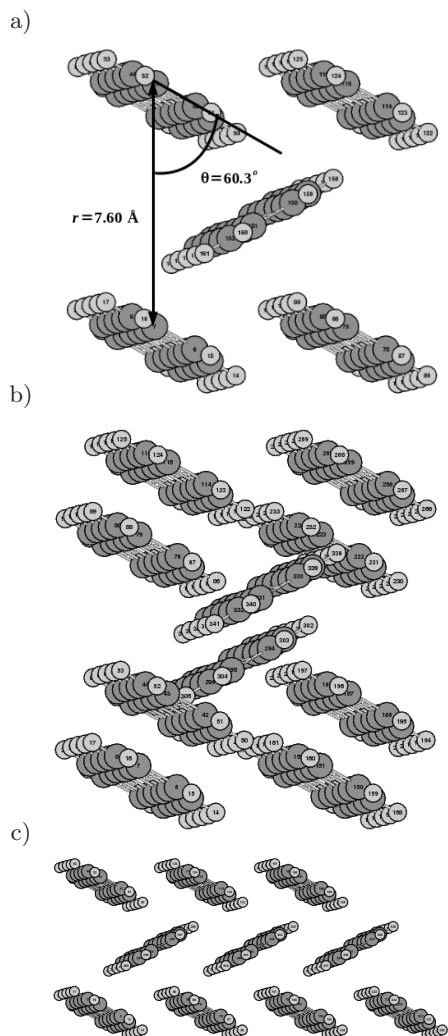


FIG. 30: Herringbone cluster models used in this work. All are portions of the x-ray crystal structure: (a) pentamer, (b) “vertical” decamer, and (c) “horizontal” decamer.

Both the TD-LDA/6-31G(d,p) and the TD-B3LYP/6-31G(d,p) calculations are red shifted compared to the thin film experiment with the TD-LDA/6-31G(d,p) red shift being quite dramatic. This is consistent with the idea that the TD-LDA/6-31G(d,p) exciton is delocalized over too many molecules while the inclusion of some HF exchange in the TD-B3LYP/6-31G(d,p) helps to increase the excitation energy by localizing the exciton over fewer molecules. The TD-DFTB calculation is in semi-quantitative agreement with the TD-B3LYP/6-31G(d,p)

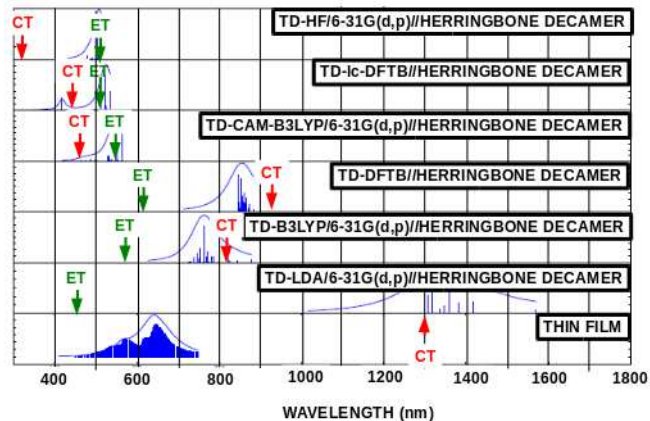


FIG. 31: Comparisons of calculations using various methods with the thin film absorption spectrum from Ref. 121. The CT and ET excitation energies were calculated from Kasha’s exciton model using Eq. (5.2).

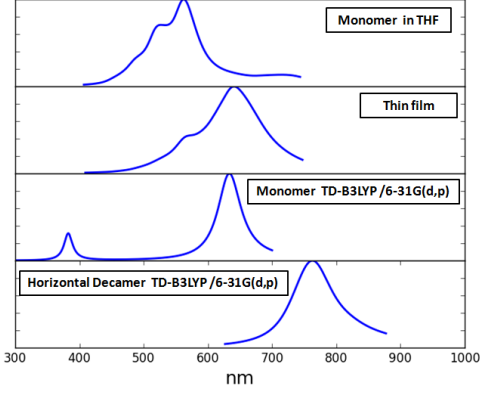
but are slightly red-shifted. In contrast, the TD-CAM-B3LYP/6-31G(d,p) and TD-HF/6-31G(d,p) calculations are blue shifted compared to the thin film experiment. The TD-lc-DFTB calculation is in semi-quantitative agreement with the TD-CAM-B3LYP/6-31G(d,p) calculation but is slightly blue shifted. It is difficult to say from this figure which of the two calculations — TD-B3LYP/6-31G(d,p) or TD-CAM-B3LYP/6-31G(d,p) — is a better description of the experiment.

The level of agreement with experiment is best judged by Fig. 32. Here we see that the TD-B3LYP/6-31G(d,p) and TD-DFTB results are in reasonable qualitative agreement with experiment. However the TD-CAM-B3LYP/6-31G(d,p) and TD-lc-DFTB results, while in good agreement with each other, do not at all provide a good description of exciton effects. We assume that this is because of the importance of CT which may be over corrected at the TD-CAM-B3LYP/6-31G(d,p) and TD-lc-DFTB levels compared with the TD-B3LYP/6-31G(d,p) and TD-DFTB levels.

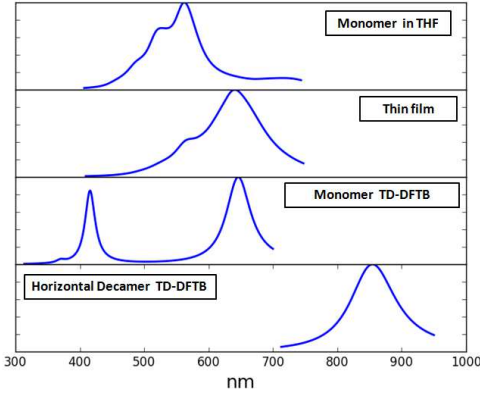
D. Re-examination of Kasha’s Model

There is some hope in the literature that you only need a single crystal plane to calculate the Davydov splitting of the crystal [131–133]. In their recent work [133], Meyenburg *et al.* give the formula [their Eq. (5) rewritten in

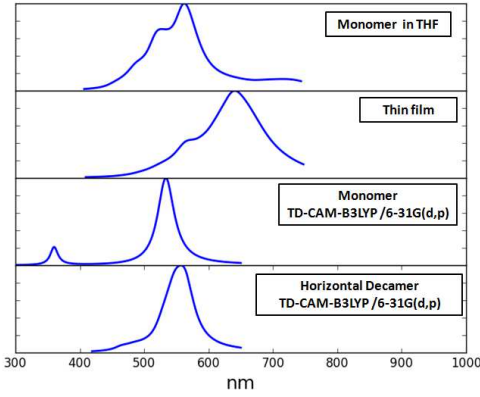
a)



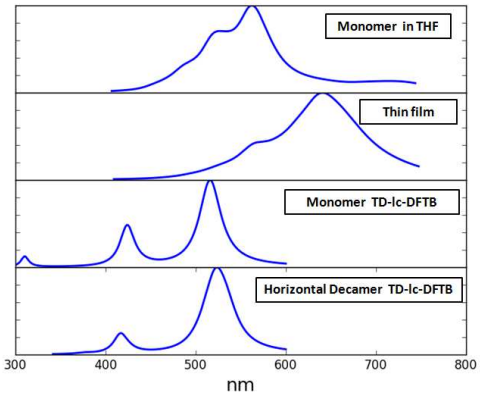
b)



c)



d)



atomic units],

$$\Delta E = \frac{2|\vec{D}|^2}{\epsilon r^3} [\cos(\phi) - 3 \cos(\alpha_1) \cos(\alpha_2)] , \quad (5.1)$$

where the angles are defined in Fig. 3 of their paper. [Equation (5.1) is a generalization of a formula given in the paper of Kasha, Rawls, and El-Bayoumi [8] (resulting in Fig. 4 of their article).] We translate this the following relationship between the DS of the herringbone model DS_{HB} and of the parallel stack model DS_{PS} :

$$DS_{HB} = DS_{PS} \left(\frac{\epsilon_{PS}}{\epsilon_{HB}} \right) \left(\frac{r_{PS}}{r_{HB}} \right)^3 \times [\cos(\phi) - 3 \cos(\alpha_1) \cos(\alpha_2)] . \quad (5.2)$$

The values $\alpha_1 = 98.19^\circ$, $\alpha_2 = 22.98^\circ$, $\phi = 58.83^\circ$, and $r = 4.835 \text{ \AA}$ were taken from the experimental crystal structure. The ratio $\epsilon_{PS}/\epsilon_{HB}$ is not something that we can really determine *a priori* and so we just use it as a fitting factor (equal to 10.64 in our calculations). We can use this, together with DS_2 to predict the DS_{HB} that we would expect from various models. These results are shown by arrows in Fig. 31. Something very remarkable has happened: The locations of the TD-IC-DFTB, TD-HF, and TD-CAM-B3LYP main peaks are well produced, as expected, by the ET peak. In contrast, the location of the TD-DFTB, TD-B3LYP, and TD-LDA main peaks has been generated unexpectedly, from the CT peak, which was expected to be relatively dark compared to the ET peak.

This leads us to take a closer look at how Kasha's exciton model works in our (TD-)DFT and (TD-)DFTB calculations. We have done this by looking at two parallel-stacked pentacenes. This corresponds to a simplification of Eq. (5.2), namely

$$\Delta E = \frac{2|\vec{D}|^2}{r^3} (1 - 3 \cos^2 \theta) , \quad (5.3)$$

with $\epsilon = 1$. Figure 33 summarizes what we expect to see on the basis of the original exciton model for excitation energies and oscillator strengths. This is a simple theory which gives simple curves. Above $\theta = 55^\circ$, the main oscillator strength is in the higher energy (lower wavelength) ET state; below $\theta = 55^\circ$, the main oscillator strength is in the lower energy (higher wavelength) ET state which has crossed the CT state. However the original theory did not anticipate avoided crossings. For the herringbone structure, $\theta \approx 60^\circ$ and the prediction is that the brighter state should be the higher wavelength

FIG. 32: Comparison of theoretical and experimental exciton

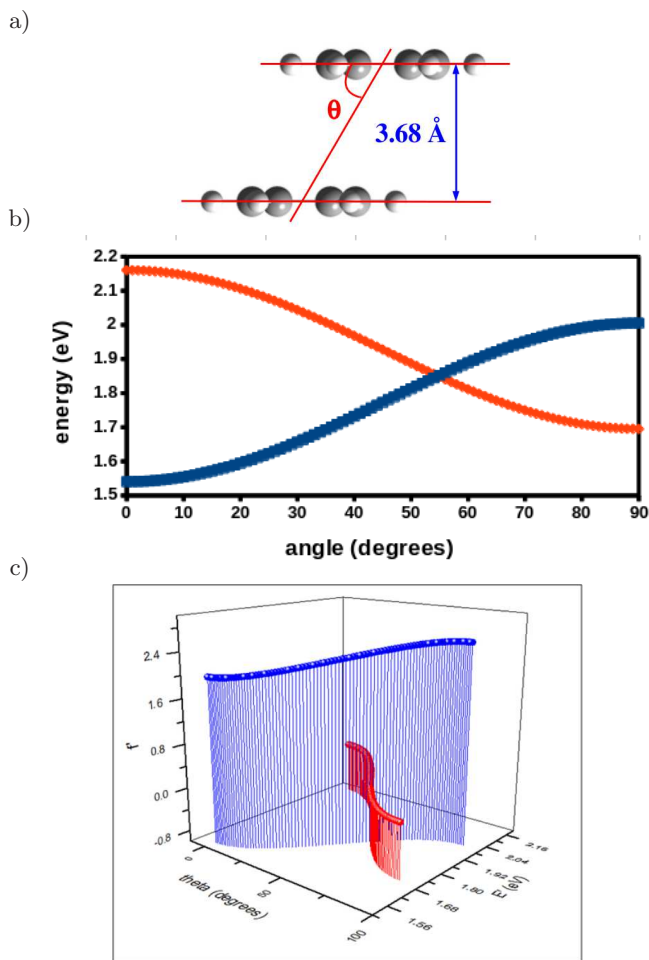


FIG. 33: Ideal Kasha figures for co-planar inclined transition dipole moments: (a) laterally shifted parallel stacked pentacene dimer, (b) Kasha plot of excitation energies as a function of the angle θ , (c) 3D plot of Kasha's model for oscillator strengths and excitation energies.

state. This is indeed what is seen in all the calculations in Fig. 31, but the assignment of the longer wavelength peak depends upon the method.

Let us turn now to Fig. 34 which shows results from our TD-B3LYP/6-31G(d,p)//B3LYP+D3/6-31G(d,p) calculations. This more realistic calculation gives more complicated results. Rather than seeing a simple crossing of energy levels at about $\theta = 55^\circ$ as in Fig. 33(b), we see evidence of configuration mixing as the oscillator strength is transferred from one state to another with maximum transfer near $\theta = 55^\circ$ (i.e., at $\theta = 45^\circ$) as the two en-

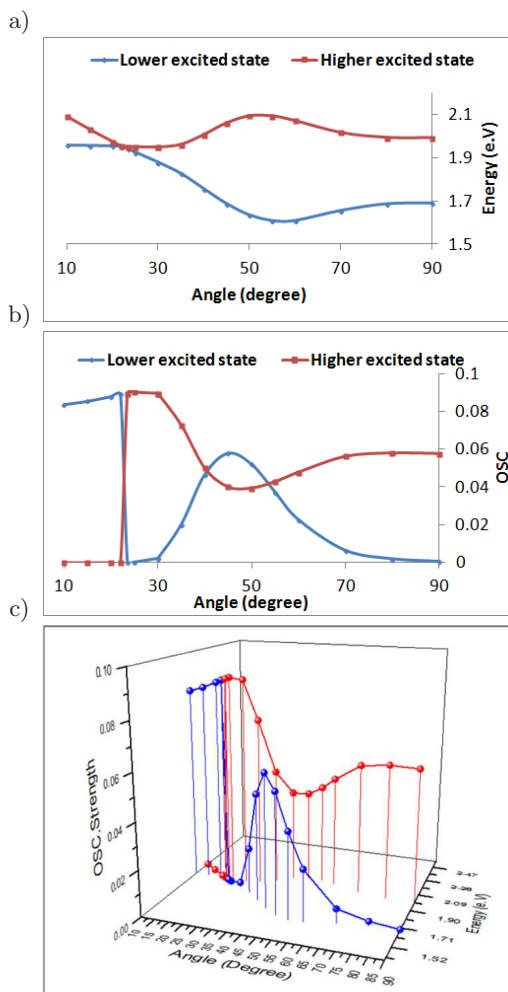


FIG. 34: TD-B3LYP/6-31G(d,p)//B3LYP+D3/6-31G(d,p) Kasha figures for co-planar inclined transition dipole moments: (a) excitation energies as a function of the angle θ , (b) 2D plot of oscillator strengths, (c) 3D plot of oscillator strengths and excitation energies,

ergy levels mix and move apart at $\theta = 55^\circ$. This seems even more clear in the 3D plot [part (c) of Fig. 34] where the two curves behave in a way very consistent with an avoided crossing of two diabatic states (one with high and one with low oscillator strength) around 50° . Later, at a much lower value of $\theta = 20^\circ$, there appears to be a real crossing, but this is of little importance for understanding the herringbone results. Comparing with the TD-DFTB, TD-B3LYP, and TD-LDA herringbone spectra in Fig. 31, we realize that the assignment of the longer

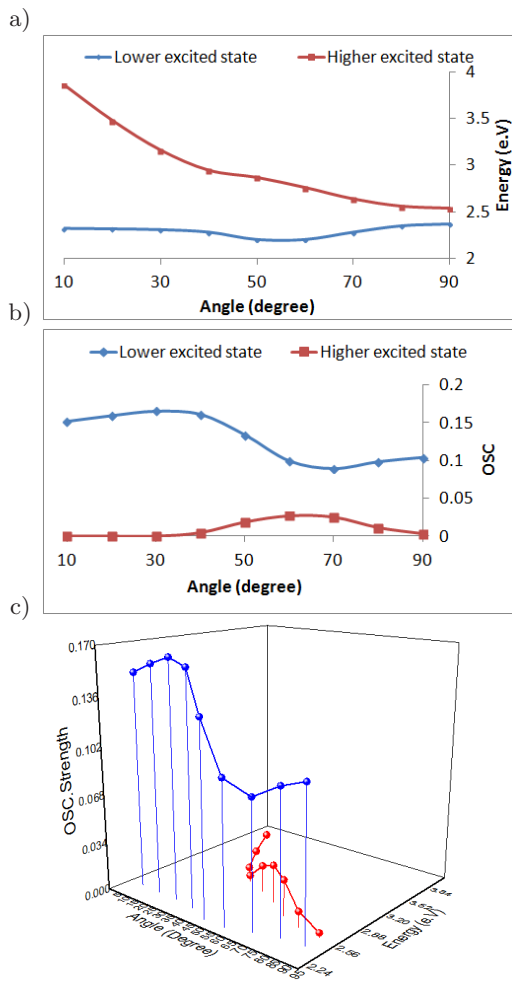


FIG. 35: TD-CAM-B3LYP/6-31G(d,p)//CAM-B3LYP+D3/6-31G(d,p) Kasha figures for co-planar inclined transition dipole moments: (a) excitation energies as a function of the angle θ , (b) 2D plot of oscillator strengths, (c) 3D plot of oscillator strengths and excitation energies,

wavelength peak as CT is misleading as most likely there is a great deal of mixing between the ET and CT states.

Figure 35 shows what happens for a RSH. In particular, TD-CAM-B3LYP/6-31G(d,p)//CAM-B3LYP+D3/6-31G(d,p) results are shown. There is also some evidence of an avoided crossing here, but the lower energy (longer wavelength) state keeps most of the oscillator strength. At $\theta = 90^\circ$, it is of ET type, but shows some mixing between CT and ET type at around $\theta = 65^\circ$. Comparing with the TD-*lc*-DFTB, TD-HF,

and TD-CAM-B3LYP herringbone spectra in Fig. 31, we realize that the assignment of the longer wavelength peak as ET is reasonable in this case.

Despite these criticisms that Kasha’s exciton model is missing many of the subtleties of our more elaborate calculations, we must conclude that the exciton model allows us to extrapolate remarkably well from intramolecular interactions between pairs of molecules to larger aggregates, but only when a RSH is used.

VI. CONCLUSION

The aggregation of dye molecules leads to additional spectral features which have long been explained by Kasha’s exciton model [8]. This model provides a simple explanation of H-bands such as those found in our calculations of parallel stacked pentacene molecules and of J-bands such as those associated with the experimentally-known herringbone structure of crystalline pentacene. We have re-examined Kasha’s exciton model in terms of state-of-the-art TD-DFT and TD-DFTB calculations. Our calculations include Grimme’s D3 dispersion correction which we confirm is absolutely necessary in order to have van der Waals binding beyond the LDA level (which, however, “accidentally” binds when an extensive-enough basis set is used). We have also included some HF exchange either in the form of the global B3LYP hybrid functional or in the form of the range-separated CAM-B3LYP hybrid functional. Corresponding TD-DFTB calculations have also been performed with DFTBABY which we find does very well at mimicking the two functionals (depending upon whether or not the long-range correction is used).

Perhaps not surprisingly we find that the hybrid functionals give better spectra than the TD-LDA. We also find that, while the TD-DFTB spectra have the structural simplicity of STO-3G minimum basis set TD-DFT spectra, the TD-DFTB spectral peak energies are placed more like the TD-DFT calculations with larger basis used in the semi-empirical parameterization. This is reassuring. However care must be taken when doing TD-DFTB calculations on aggregates to do them size consistently or results can be misleading — that is, the size of the active space must increase in proportion to the number of molecules in the aggregate.

On the other hand, Fig. 32 is definitely telling us that the Davydov splitting for the herringbone model is reasonable and close to the experimental value at the TD-B3LYP and TD-DFTB levels, even if the spectral peaks

are shifted, but that the Davydov splitting is practically nonexistent and therefore wrong at the CAM-TD-B3LYP and TD-*lc*-DFTB levels. For this reason, we cannot recommend using either of these latter two approaches for calculating excitonic effects on the spectra of poly-oligocenes and recommend instead the use of TD-B3LYP or TD-DFTB carefully carried out on aggregates.

Also, in light of arguments regarding the extent and nature of exciton delocalization (e.g., Refs. 43, 134), it is interesting that our analysis shows that a more sophisticated version of Kasha’s exciton model, based only on nearest neighbor interactions but including both ET and CT as well as avoided crossings, works very well. In contrast, Kasha’s original model fails for displaced parallel pentacene dimers unless RSHs are used because of failure to take proper account of avoided crossings.

Acknowledgments

This work is supported, in part, by the ORGAVOLT (ORGANic solar cell VOLTage by numerical computation) Grant ANR-12-MONU-0014-02 of the French *Agence Nationale de la Recherche (ANR) 2012 Programme Modèles Numériques*. Ala Aldin M. H. M. Darghouth would like to thank the French and Iraq governments for support through a Campus France scholarship. Gabriela Calinao Correa was an American iREU (International Research Experience for Undergraduates) scholar who acknowledges support from Chemistry (CHE) Grant Number 1263336 of the American National Science Foundation (NSF) and the Labex Arcane ANR-11-LABX-0003-01 French Grant. Mark E. Casida and Ala Aldin M. H. M. Darghouth would like to acknowledge helpful discussions with Mathias Rapacioli. Mark E. Casida and Ala Aldin M. H. M. Darghouth would also like to acknowledge a useful trip to Würzburg funded by the German GRK 2112 Project “Biradicals.”

Author Contributions

This project began with a two month research project under the direction of Mark E. Casida during the summer of 2013 when Sacha Juillard, then a first-year Masters student in Chemistry, explored the possibilities for using DFTB to model polymers in organic photovoltaic cells. The project continued with calculations carried out by Ala Aldin M. H. M. Darghouth as part of his PhD project with Mark E. Casida. Major coding was

done by Alexander Humeniuk and by Roland Mitrić in their TD-DFTB program. Gabriela Calinao Correa contributed to expanding the understanding of those of us in Grenoble of the TD-DFTB code via her work analysing and applying DFTBABY. The bulk of the manuscript writing was done by Mark E. Casida with contributions from Gabriela Calinao Correa and major contributions from Ala Aldin M. H. M. Darghouth.

Conflicts of Interest

The authors declare no conflict of interest.

Abbreviations

For the reader’s convenience, we have collected together the abbreviations used in this paper:

- AO** Atomic orbital.
- B88** Becke’s 1988 exchange GGA
- BS** Band structure.
- BSE** Bethe-Salpeter equation.
- CAM** Coulomb attenuated model.
- CAO** Crystal atomic orbital.
- CIS** Configuration interaction with single excitations.
- CMO** Crystal molecular orbital.
- CT** Charge transfer.
- D3** Grimme’s 3-parameter vdW energy correction.
- DFT** Density-functional theory.
- DFTB** Density-functional tight binding.
- DS** (= ET - CT) Davydov splitting.
- ERI** Electron repulsion integral.
- ET** Energy transfer.
- FR** Frenkel.
- GGA** Generalized gradient approximation.
- H-bands** Hypsochromatic bands, high energy spectral peaks due to aggregation.

H Highest-occupied molecular orbital.	MO Molecular orbital.
H-n n th level below the HOMO.	NTO Natural transition orbital.
HEG Homogeneous electron gas.	PES Potential energy surface (also, somewhat abusively, used to mean a potential energy curve).
HF Hartree-Fock.	RSH Range-separated hybrid.
HOMO Highest-occupied molecular orbital.	SCC Self-consistent charge.
IUPAC International Union of Pure and Applied Chemistry.	sr Short range.
J-bands Jelly bands (also known as Scheibe bands), low energy spectral peaks due to aggregation.	TD Time-dependent
L Lowest-unoccupied molecular orbital.	TDA Tamm-Dancoff approximation.
L+n n th level above the LUMO.	TD-DFT Time-dependent density-functional theory.
LAO Localized atomic orbital.	TD-DFTB Time-dependent density-functional tight binding.
LDA Local density approximation.	THF Tetrahydrofuran.
LE Local excitation.	TOTEM Two-orbital two-electron model.
LMO Localized molecular orbital.	(TOTEM)^{n} n stacked TOTEMs.
lr Long range.	vdW Van der Waals.
LRC Long-range corrected.	WM Wannier-Mott.
LUMO Lowest-unoccupied molecular orbital.	xc Exchange correlation.
LYP Lee-Yang-Parr correlation GGA.	
MBPT Many-body perturbation theory.	

-
- [1] Present address: Doctoral student in the Department of Materials Science, Cornell University, Ithaca, New York.
- [2] M. E. Casida and M. Huix-Rotllant, *Annu. Rev. Phys. Chem.* **63**, 287 (2012), [Progress in Time-Dependent Density-Functional Theory](#).
- [3] M. E. Casida and M. Huix-Rotllant, in *Density-Functional Methods for Excited States*, edited by N. Ferré, M. Filatov, and M. Huix-Rotllant (Springer, 2015), Topics in Current Chemistry, [Many-Body Perturbation Theory \(MBPT\) and Time-Dependent Density-Functional Theory \(TD-DFT\): MBPT Insights About What is Missing in, and Corrections to, the TD-DFT Adiabatic Approximation](#).
- [4] S. Grimme, J. Antony, S. Ehrlich, and H. Krieg, *J. Chem. Phys.* **132**, 154104 (2010), [A consistent and accurate *ab initio* parameterization of density functional dispersion correction \(DFT-D\) for the 94 elements H-Pu](#).
- [5] R. S. Knox, [Theory of Excitons](#), vol. 5 of *Solid State Physics* (Academic Press, New York, 1963).
- [6] V. May and O. Kühn, [Charge and Energy Transfer Dynamics in Molecular Systems: A Theoretical Introduction](#) (Wiley-VCH, Berlin, 2000).
- [7] M. Kasha, *Rev. Mod. Phys.* **31**, 162 (1959), [Relation between Exciton Bands and Conduction Bands in Molecular Lamellar Systems](#).
- [8] M. Kasha, H. R. Rawls, and A. El-Bayoumi, *Pure Appl. Chem.* **11**, 371 (1965), [The exciton model in molecular spectroscopy](#).
- [9] H. van Amerongen, L. Valkunas, and R. van Grondelle, [Photosynthetic Excitons](#) (World Scientific, Singapore, 2000).

- [10] J. Frenkel, Phys. Rev. **37**, 17 (1931), [On the Transformation of light into Heat in Solids. I.](#)
- [11] J. Frenkel, Phys. Rev. **37**, 1276 (1932), [On the Transformation of light into Heat in Solids. II.](#)
- [12] G. H. Wannier, Phys. Rev. **52**, 191 (1937), [The structure of electronic excitation levels in insulating crystals.](#)
- [13] A. S. Davydov, Sov. Phys. Usp. **7**, 145 (1964), [The theory of molecular excitons.](#)
- [14] A. S. Davydov, Ukr. J. Phys. **53**, 65 (2008), [Theory of Absorption Spectra of Molecular Crystals](#), translated and reprinted from *Zh. Eksp. Teor. Fiz.* **18**, 210 (1948).
- [15] D. Möbius, Adv. Mat. **7**, 437 (1995), [Scheibe aggregates.](#)
- [16] E. E. Jelley, **138**, 1009 (1936), [Spectral Absorption and Fluorescence of Dyes in the Molecular State.](#)
- [17] E. E. Jelley, **139**, 631 (1937), [Molecular, Nematic and Crystal States of I'-Diethyl- \$\psi\$ -Cyanine Chloride.](#)
- [18] G. Scheibe, Angew. Chem. **50**, 212 (1937), [Über die Veränderlichkeit der Absorptionsspektren in Lösungen und die Nebenvalezen als ihre Ursache.](#)
- [19] F. Würthner, T. E. Kaiser, and C. R. Saha-Möller, Angew. Chem. Int. Ed. **50**, 3376 (2011), [J-aggregates: From serendipitous discover to supramolecular engineering of functional dye materials.](#)
- [20] P. Cudazzo, F. Sottile, A. Rubio, and M. Gatti, J. Phys.: Condens. Matter **27**, 113204 (2015), [Topical Review: Exciton dispersion in molecular solids.](#)
- [21] A. Dreuw, J. L. Weisman, and M. Head-Gordon, J. Chem. Phys. **119**, 2943 (2003), [Long-range charge-transfer excited states in time-dependent density functional theory require non-local exchange.](#)
- [22] D. J. Tozer, R. D. Amos, N. C. Handy, B. O. Roos, and L. Serrano-Andrés, Mol. Phys. **97**, 859 (1999), [Does density functional theory contribute to the understanding of excited states of unsaturated organic compounds?](#)
- [23] M. J. G. Peach, P. Benfield, T. Helgaker, and D. J. Tozer, J. Chem. Phys. **128**, 044118 (2008), [Excitation energies in density functional theory: an evaluation and a diagnostic test.](#)
- [24] M. J. G. Peach and D. J. Tozer, J. Mol. Struct.: THEOCHEM **914**, 110 (2009), [Illustration of a TDDFT spatial overlap diagnostic by basis function exponent scaling.](#)
- [25] M. J. G. Peach, C. R. L. Sueur, K. Rüüd, M. Guillaume, and D. J. Tozer, Phys. Chem. Chem. Phys. **11**, 4465 (2009), [TDDFT diagnostic testing and functional assessment for triazene chromophores.](#)
- [26] T. S. Kuhlman, K. V. Mikkelsen, K. B. Møller, and T. L. Sølling, Chem. Phys. Lett. **478**, 127 (2009), [Charge-resonance excitations in symmetric molecules — Comparison of linear response DFT with CC3 for the excited states of a model dimer.](#)
- [27] P. Wiggins, J. A. G. Williams, and D. J. Tozer, J. Chem. Phys. **131**, 091101 (2009), [Excited state surfaces in density functional theory: A new twist on an old problem.](#)
- [28] A. D. Dwyer and D. J. Tozer, Phys. Chem. Chem. Phys. **12**, 2816 (2010), [Effect of chemical change on TDDFT accuracy: orbital overlap perspective of the hydrogenation of retinal.](#)
- [29] S. S. Leang, F. Zahariev, and M. S. Gordon, J. Chem. Phys. **136**, 104101 (2012), [Benchmarking the performance of time-dependent density functional methods.](#)
- [30] G. Vignale and W. Kohn, Phys. Rev. Lett. **77**, 2037 (1996), [Current-dependent exchange-correlation potential for dynamical linear response theory.](#)
- [31] F. Sottile, M. Marsili, V. Olevano, and L. Reining, Phys. Rev. B **76**, 161103(R) (2007), [Efficient *ab initio* calculations of bound and continuum excitons in the absorption spectra of semiconductors and insulators.](#)
- [32] S. Sharma, J. K. Dewhurst, A. Sanna, and E. K. U. Gross, Phys. Rev. Lett. **107**, 186401 (2011), [Bootstrap Approximation for the Exchange-Correlation Kernel of Time-Dependent Density-Functional Theory.](#)
- [33] V. Turkowski, A. Leonardo, and C. A. Ulrichs, Phys. Rev. B **79**, 233201 (2009), [Time-dependent density-functional approach for exciton binding energies.](#)
- [34] Z. Yang and C. A. Ullrich, Phys. Rev. B **87**, 195204 (2013), [Direct calculation of exciton binding energies with time-dependent density-functional theory.](#)
- [35] C. A. Ullrich and Z. Yang, in *Density-Functional Methods for Excited States* (Springer, New York, 2016), vol. 368 of *Topics in Current Chemistry*, p. 185, [Excitons in Time-Dependent Density-Functional Theory.](#)
- [36] S. Kümmel, Adv. Energy Mat. **7**, 1700440 (2017), [Charge-transfer excitations: A challenge for time-dependent density functional theory that has been met.](#)
- [37] B. M. Wong and T. H. Hsieh, J. Chem. Theory. Comput. **6**, 3704 (2010), [Optoelectronic and Excitonic Properties of Oligoacenes: Substantial Improvements from Range-Separated Time-Dependent Density Functional Theory.](#)
- [38] C. R. Jacob and J. Neugebauer, WIREs Comp. Molec. Sci. **4**, 325 (2014), [Subsystem density-functional theory.](#)
- [39] P. Ramos and M. Pavenello, Phys. Chem. Chem. Phys. **18**, 21172 (2016), [Constrained subsystem density functional theory.](#)
- [40] M. E. Casida and T. A. Wesolowski, Int. J. Quant. Chem. **96**, 577 (2004), [Generalization of the Kohn-Sham Equations with Constrained Electron Density \(KSCED\) Formalism and its Time-Dependent Response Theory Formulation.](#)
- [41] A. A. Kocherzhenko, X. A. S. Vasquez, J. M. Milanese, and C. M. Isborn, J. Chem. Theory. Comput. **13**, 3787 (2017), [Absorption spectra for disordered aggregates of chromophores using the exciton model.](#)
- [42] J. E. Anthony, Angew. Chem. Int. Ed. **47**, 452 (2008), [The Larger Acenes: Versatile Organic Semiconductors.](#)
- [43] P. M. Zimmerman, F. Bell, D. Casanova, and M. Head-Gordon, J. Am. Chem. Soc. **133**, 19944 (2009), [Mechanism for singlet fission in pentacene and tetracene from single exciton to two triplets.](#)
- [44] R. S. Mulliken, J. Chem. Phys. **23**, 1997 (1955), [Report](#)

- on Notation for the Spectra of Polyatomic Molecules.
- [45] R. S. Mulliken, *J. Chem. Phys.* **24**, 1118(E) (1956), [Erratum : Report on Notation for the Spectra of Polyatomic Molecules](#).
- [46] J. Koutecký and J. Paldus, *Theoret. chim. Acta (Berl.)* **1**, 268 (1963), [A study of interaction of two ethylene molecules by the semiempirical complete configuration interaction method in \$\pi\$ -electron approximation](#).
- [47] G. D. Scholes and K. P. Ghiggino, *J. Chem. Phys.* **101**, 1251 (1994), [Rate expressions for excitation transfer I. Radiationless transition theory perspective](#).
- [48] R. D. Harcourt, G. D. Scholes, and K. P. Ghiggino, *J. Chem. Phys.* **101**, 10521 (1994), [Rate expressions for excitation transfer II. Electronic considerations of direct and through-configuration exciton resonance interactions](#).
- [49] G. D. Scholes, R. D. Harcourt, and K. P. Ghiggino, *J. Chem. Phys.* **102**, 9574 (1995), [Rate expressions for excitation transfer III. An ab initio study of electronic factors in excitation transfer and exciton resonance interactions](#).
- [50] P. Hohenberg and W. Kohn, *Phys. Rev.* **136**, B864 (1964), [Inhomogeneous electron gas](#).
- [51] W. Kohn and L. J. Sham, *Phys. Rev.* **140**, A1133 (1965), [Self-consistent equations including exchange and correlation effects](#).
- [52] R. G. Parr and W. Yang, *Density-Functional Theory of Atoms and Molecules* (Oxford University Press, New York, 1989).
- [53] R. M. Dreizler and E. K. U. Gross, *Density Functional Theory, An Approach to the Quantum Many-Body Problem* (Springer-Verlag, New York, 1990).
- [54] W. Koch and M. C. Holthausen, *A Chemist's Guide to Density Functional Theory* (Wiley-VCH, New York, 2000).
- [55] P. A. M. Dirac, *Proc. Cambridge Phil. Roy. Soc.* **26**, 376 (1930), [Note on exchange phenomena in the Thomas-Fermi atom](#).
- [56] S. H. Vosko, L. Wilk, and M. Nusair, *Can. J. Phys.* **58**, 1200 (1980), [Accurate spin-dependent electron liquid correlation energies for local spin density calculations: a critical analysis](#).
- [57] A. D. Becke, *Phys. Rev. A* **38**, 3098 (1988), [Density-functional exchange-energy approximation with correct asymptotic behavior](#).
- [58] L. Fan and T. Ziegler, *J. Chem. Phys.* **94**, 6057 (1991), [The influence of self-consistency on nonlocal density functional calculations](#).
- [59] J. P. Perdew, J. A. Chevary, S. H. Vosko, K. A. Jackson, M. R. Pederson, D. J. Singh, and C. Fiolhais, *Phys. Rev. B* **46**, 6671 (1992), [Atoms, molecules, solids, and surfaces: Applications of the generalized gradient approximation for exchange and correlation](#).
- [60] J. P. Perdew, J. A. Chevary, S. H. Vosko, K. A. Jackson, M. R. Pederson, D. J. Singh, and C. Fiolhais, *Phys. Rev. B* **48**, 4978 (1993), [Erratum: "Atoms, molecules, solids, and surfaces: Applications of the generalized gradient approximation for exchange and correlation"](#).
- [61] J. P. Perdew, K. Burke, and Y. Wang, *Phys. Rev. B* **54**, 16533 (1996), [Generalized gradient approximation for the exchange-correlation hole of a many-electron system](#).
- [62] J. P. Perdew, K. Burke, and Y. Wang, *Phys. Rev. B* **57**, 14999 (1996), [Erratum: "Generalized gradient approximation for the exchange-correlation hole of a many-electron system"](#).
- [63] C. Lee, W. Yang, and R. G. Parr, *Phys. Rev. B* **37**, 785 (1988), [Development of the Colle-Salvetti correlation energy formula into a functional of the electron density](#).
- [64] A. D. Becke, *J. Chem. Phys.* **98**, 1372 (1993), [A new mixing of Hartree-Fock and local density functional theories](#).
- [65] P. M. W. Gill, *Aust. J. Chem.* **54**, 661 (2001), [Obituary: Density-functional theory \(1927-1993\)](#).
- [66] [Becke3LYP Method References and General Citation Guidelines](#), *Gaussian NEWS*, v. 5, no. 2, summer 1994.
- [67] T. Yanai, D. P. Tew, and N. C. Handy, *Chem. Phys. Lett.* **393**, 51 (2004), [A new hybrid exchange-correlation functional using the Coulomb-attenuating method \(CAM-B3LYP\)](#).
- [68] H. Iikura, T. Tsuneda, T. Yanai, and K. Hirao, *J. Chem. Phys.* **115**, 3540 (2001), [A long-range correction scheme for generalized-gradient-approximation exchange functionals](#).
- [69] E. Runge and E. K. U. Gross, *Phys. Rev. Lett.* **52**, 997 (1984), [Density-functional theory for time-dependent systems](#).
- [70] M. A. L. Marques, C. Ullrich, F. Nogueira, A. Rubio, and E. K. U. Gross, eds., *Time-Dependent Density-Functional Theory*, vol. 706 of *Lecture Notes in Physics* (Springer, Berlin, 2006).
- [71] M. A. L. Marques, N. Maitra, F. Nogueira, E. K. U. Gross, and A. Rubio, eds., *Fundamentals of Time-Dependent Density-Functional Theory*, vol. 837 of *Lecture Notes in Physics* (Springer, Berlin, 2011).
- [72] G. D. Mahan and K. R. Subbaswamy, *Local Density Theory of Polarizability* (Plenum, New York, 1990).
- [73] C. A. Ullrich, *Time-Dependent Density-Functional Theory* (Oxford University Press, New York, 2012).
- [74] K. Burke, J. Werschnik, and E. K. U. Gross, *J. Chem. Phys.* **123**, 062206 (2005), [Time-dependent density functional theory: Past, present, and future](#).
- [75] M. E. Casida, *J. Mol. Struct. (Theochem)* **914**, 3 (2009), [Review: Time-Dependent Density-Functional Theory for Molecules and Molecular Solids](#).
- [76] D. Jacquemin, V. Wathelet, E. A. Perpète, and C. Adamo, *J. Chem. Theory Comput.* **5**, 2420 (2009), [Extensive TD-DFT benchmark: Singlet-excited states of organic molecules](#).
- [77] C. Adamo and D. Jacquemin, *Chem. Soc. Rev.* **42**, 845 (2013), [The calculations of excited-state properties with time-dependent density functional theory](#).
- [78] A. D. Laurent and D. Jacquemin, *Int. J. Quant. Chem.*

- 113**, 2019 (2013), [TD-DFT benchmarks: A review](#).
- [79] N. T. Maitra, *J. Chem. Phys.* **144**, 220901 (2016), [Perspective: Fundamental aspects of time-dependent density functional theory](#).
- [80] M. E. Casida, in *Recent Advances in Density Functional Methods, Part I*, edited by D. P. Chong (World Scientific, Singapore, 1995), p. 155, [Time-dependent density-functional response theory for molecules](#).
- [81] X. Gonze and M. Scheffler, *Phys. Rev. Lett.* **82**, 4416 (1999), [Exchange and correlation kernels at the resonance frequency: implications for excitation energies in density-functional theory](#).
- [82] M. Swart, F. M. Bickelhaupt, and M. Duran, [DFT2016 poll](#), <http://www.marcelswart.eu/dft-poll/news2016.pdf>, last accessed: 21 January 2018.
- [83] J. A. Pople and D. L. Beveridge, *Approximate Molecular Orbital Theory* (McGraw-Hill, New York, 1970).
- [84] T. Bredow and K. Jug, *Theor. Chem. Acc.* **113**, 1 (2005), [Theory and range of modern semiempirical molecular orbital methods](#).
- [85] A. Horsfield, *Phys. Status Solidi B* **249**, 231 (2012), [Where does tight binding go from here?](#)
- [86] P. Koskinen and V. Mönkinen, *Comput. Mater. Sci.* **47**, 237 (2009), [Density-functional tight-binding for beginners](#).
- [87] A. Oliveira, G. Seifert, T. Heine, and H. Duarte, *J. Braz. Chem. Soc.* **20**, 1193 (2009), [Density-functional based tight-binding: An approximate DFT method](#).
- [88] M. Elstner and G. Seifert, *Philos. Trans. R. Soc. A* **372**, 20120483 (2014), [Density functional tight binding](#).
- [89] D. Porezag, T. Frauenheim, T. Köhler, G. Seifert, and R. Kaschner, *Phys. Rev. B* **51**, 12947 (1995), [Construction of tight-binding-like potentials on the basis of density-functional theory: Application to carbon](#).
- [90] R. Hoffmann, *J. Chem. Phys.* **39**, 1397 (1963), [An extended Hückel theory. I. Hydrocarbons](#).
- [91] R. Hoffmann, *J. Chem. Phys.* **40**, 2745 (1964), [An extended Hückel theory. II. \$\sigma\$ orbitals in the azines](#).
- [92] R. Hoffmann, *J. Chem. Phys.* **40**, 2474 (1964), [An extended Hückel theory. III. Compounds of boron and nitrogen](#).
- [93] R. Hoffmann, *J. Chem. Phys.* **40**, 2480 (1964), [An extended Hückel theory. IV. Carbonium ions](#).
- [94] M. Elstner, D. Porezag, G. Jungnickel, J. Elsner, M. Haugk, T. Frauenheim, S. Suhai, and G. Seifert, *Phys. Rev. B* **58**, 7260 (1998), [Self-consistent-charge density-functional tight-binding method for simulations of complex materials properties](#).
- [95] M. Gaus, Q. Cui, and M. Elstner, *J. Chem. Theory Comput.* **7**, 931 (2011), [DFTB3: Extension of the self-consistent-charge density-functional tight-binding method \(SCC-DFTB\)](#).
- [96] R. S. Mulliken, *Journal de Chimie Physique et de Physico-Chimie Biologique* **497** (1949), [Report on Molecular Orbital Theory](#).
- [97] T. Frauenheim, G. Seifert, M. Elstner, T. Niehaus, C. Kohler, M. Amkreutz, M. Sternberg, Z. Hajnal, A. D. Carlo, and S. Suhai, *J. Phys.: Condens. Matter* **14**, 3015 (2002), [Atomistic simulations of complex materials: ground-state and excited-state properties](#).
- [98] R. Pariser, *J. Chem. Phys.* **21**, 568 (1953), [An improvement on the \$\pi\$ -electron approximation in LCAO MO theory](#).
- [99] A. M. H. M. Darghouth, M. E. Casida, W. Taouali, K. Alimi, M. P. Ljungberg, P. Koval, D. Sánchez-Portal, and D. Foerster, *Computation* **3**, 616 (2015), [Assessment of density-functional tight-binding ionization potentials and electron affinities of molecules of interest for organic solar cells against first-principles *GW* calculations](#).
- [100] T. Niehaus and F. Della Sala, *Phys. Status Solidi B* **2**, 237 (2012), [Range separated functionals in the density functional tight-binding method](#).
- [101] V. Lutsker, B. Aradi, and T. A. Niehaus, *J. Chem. Phys.* **143**, 184107 (2015), [Implementation and benchmark of a long-range corrected functional in the density functional based tight-binding method](#).
- [102] V. Q. Vuong, J. A. Kuriappan, M. Kubillus, J. J. Kranz, T. Mast, T. A. Niehaus, S. Irle, and M. Elstner, *J. Chem. Theory Comput.* **14**, 115 (2018), [Parameterization and benchmark of long-range corrected DFTB2 for organic molecules](#).
- [103] A. Humeniuk and R. Mitrić, *J. Chem. Phys.* **143**, 134120 (2015), [Long-range correction for tight-binding TD-DFT](#).
- [104] A. Humeniuk and R. Mitrić, *Comp. Phys. Comm.* **221**, 174 (2017), [DFTBABY: A software package for non-adiabatic molecular dynamics simulations based on long-ranged corrected tight-binding TD-DFT\(B\)](#).
- [105] T. Niehaus, S. Suhai, F. Della Sala, R. Lugli, M. Elstner, G. Seifert, and T. Frauenheim, *Phys. Rev. B* **63**, 085108 (2001), [Tight-binding approach to time-dependent density-functional response theory](#).
- [106] D. Heringer, T. A. Niehaus, M. Wanko, and T. Frauenheim, *J. Comput. Chem.* **28**, 2589 (2007), [Analytical excited state forces for the time-dependent density-functional tight-binding method](#).
- [107] T. A. Niehaus, *J. Molec. Struct.: THEOCHEM* **914**, 38 (2009), [Approximate time-dependent density functional theory](#).
- [108] T. A. Niehaus, S. Suhai, F. D. Sala, P. Lugli, M. Elstner, G. Seifert, and T. Frauenheim, *Phys. Rev. B* **63**, 085108 (2001), [Tight-binding approach to time-dependent density-functional response theory](#).
- [109] F. Trani, G. Scalmani, G. Zheng, I. Carnimeo, M. Frisch, and V. Barone, *J. Chem. Theory Comput.* **7**, 3304 (2011), [Time-dependent density-functional tight binding: New formulation and benchmark of excited states](#).
- [110] M. J. Frisch, G. W. Trucks, H. B. Schlegel, G. E. Scuseria, M. A. Robb, J. R. Cheeseman, G. Scalmani, V. Barone, B. Mennucci, G. A. Petersson, et al., [GAUS-](#)

- SIAN09 Revision D.01, Gaussian Inc. Wallingford CT 2009.
- [111] W. J. Hehre, L. Radom, P. v. R. Schleyer, and J. A. Pople, *Ab Initio Molecular Orbital Theory* (John Wiley and Sons, New York, 1986).
- [112] W. J. Hehre, R. F. Stewart, and J. A. Pople, *J. Chem. Phys.* **51**, 2657 (1969), [SelfConsistent MolecularOrbital Methods. I. Use of Gaussian Expansions of SlaterType Atomic Orbitals.](#)
- [113] W. J. Hehre, R. Ditchfield, R. F. Stewart, and J. A. Pople, *J. Chem. Phys.* **52**, 2769 (1970), [SelfConsistent Molecular Orbital Methods. IV. Use of Gaussian Expansions of SlaterType Orbitals. Extension to SecondRow Molecules.](#)
- [114] R. Ditchfield, W. J. Hehre, and J. A. Pople, *J. Chem. Phys.* **54**, 724 (1971), [SelfConsistent MolecularOrbital Methods. IX. An Extended GaussianType Basis for MolecularOrbital Studies of Organic Molecules.](#)
- [115] W. J. Hehre, R. Ditchfield, and J. A. Pople, *J. Chem. Phys.* **56**, 2257 (1972), [SelfConsistent Molecular Orbital Methods. XII. Further Extensions of GaussianType Basis Sets for Use in Molecular Orbital Studies of Organic Molecules.](#)
- [116] P. C. Harihan and J. A. Pople, *Chem. Phys. Lett.* **16**, 217 (1972), [The effect of \$d\$ -functions on molecular orbital energies for hydrocarbons.](#)
- [117] D. L. Dorset and M. P. McCourt, *Acta Crystallogr. Sect. A* **50**, 344 (1994), [Disorder and the molecular packing of \$C_{60}\$ buckminsterfullerene: A direct electron-crystallographic analysis.](#)
- [118] S. Schiefer, M. Huth, A. Dobrinevski, and B. Nickel, *J. Am. Chem. Soc.* **129**, 10316 (2007), [Determination of the Crystal Structure of Substrate-Induced Pentacene Polymorphs in Fiber Structured Thin Films.](#)
- [119] A. Rauk, [Interactive Simple Hückel Molecular Orbital \(SHMO\) Theory Calculator](#), <http://www.ucalgary.ca/rauk/shmo> (accessed 22 July 2016).
- [120] J. A. Huwaldt, [PLOT DIGITIZER, version 2.6.8](#), [//http://plotdigitizer.sourceforge.net/](http://plotdigitizer.sourceforge.net/) (accessed 28 June 2017).
- [121] A. Maliakal, K. Raghavachari, H. Katz, E. Chandross, and T. Siegrist, *Chem. Mater.* **16**, 4980 (2004), [Photochemical stability of pentacene and a substituted pentacene in solution and in thin films.](#)
- [122] E. Heinecke, D. Hartmann, R. Müller, and A. Hese, *J. Chem. Phys.* **109**, 906 (1998), [Laser spectroscopy of free pentacene molecules \(I\): The rotational structure of the vibrationless \$S_1 \leftarrow S_0\$ transition.](#)
- [123] T. M. Halasinski, D. M. Hudgins, F. Salama, L. J. Al-lamandola, and T. Bally, *J. Chem. Phys. A* **104**, 7484 (2000), [Electronic absorption spectra of neutral pentacene \(\$C_{22}H_{14}\$ \) and its positive and negative ions in Ne, Ar, and Kr matrices.](#)
- [124] M. S. Alam, J. Lin, and M. Saito, *Jap. J. Appl. Phys.* **50**, 080213 (2011), [First-principles calculation of the interlayer distance of the two-layer graphene.](#)
- [125] M. L. Tiago, J. E. Northrup, and S. G. Louie, *Phys. Rev. B* **67**, 115212 (2003), [Ab initio calculation of the electronic and optical properties of solid pentacene.](#)
- [126] L. Sebastian, G. Weiser, and H. Bässler, *Chem. Phys.* **61**, 125 (1981), [Charge transfer transitions in solid tetracene and pentacene studied by electroabsorption.](#)
- [127] N. J. Hestand, H. Yamagata, B. Xu, D. Sun, Y. Zhong, A. R. Harutyunyan, G. Chen, H.-L. Dai, Y. Rao, and F. C. Spano, *J. Phys. Chem.* **119**, 22137 (2015), [Polarized absorption in crystalline pentacene: Theory vs experiment.](#)
- [128] C. Ambrosch-Draxl, D. Nabok, P. Puschnig, and C. Meisenbichler, *New J. Phys.* **11**, 125010 (2009), [The role of polymorphism in organic thin films: oligoacenes investigated from first principles.](#)
- [129] P. Cudazzo, M. Gatti, A. Rubio, and F. Sottile, *Phys. Rev. B* **88**, 195152 (2013), [Frenkel versus charge-transfer exciton dispersion in molecular crystals.](#)
- [130] S. Sharifzadeh, P. Darancet, L. Kronk, and J. B. Neaton, *J. Phys. Chem. Lett.* **4**, 2197 (2013), [Low-energy charge-transfer excitons in organic solids from first-principles: The case of pentacene.](#)
- [131] M. R. Philpott, *J. Chem. Phys.* **58**, 588 (1973), [Planewise summation of point dipole-dipole interactions for some aromatic hydrocarbon crystals.](#)
- [132] H. Yamagata, J. Norton, E. Hontz, Y. Olivier, D. Bejonne, J. L. Brédas, R. J. Silbey, and F. C. Spano, *J. Chem. Phys.* **134**, 204703 (2011), [The nature of singlet excitons in oligoacene molecular crystals.](#)
- [133] I. Meyenburg, T. Breuer, A. Karthäuser, S. Chatterjee, G. Witte, and W. Heimbrodt, *Phys. Chem. Chem. Phys.* **18**, 3825 (2016), [Temperature-resolved optical spectroscopy of pentacene polymorphs: variation of herringbone angles in single-crystals and interface-controlled thin films.](#)
- [134] S. A. Mewes, F. Plasser, and A. Dreuw, *J. Phys. Chem. Lett.* **8**, 1205 (2017), [Universal exciton size in organic polymers is determined by nonlocal exchange in time-dependent density functional theory.](#)